# The effects of macro and micro road texture on tyre simulations

Department of Mechanical and Aeronautical Engineering

University of Pretoria

O Scholtz

11135582

Supervisor: Prof P.S. Els

2018

# Abstract

The tyre contact patch is important to vehicle dynamics analysis since this is where the tyre-road interaction forces originate. If the contact patch mechanism is understood in depth and can be simulated accurately, it could improve various aspects of vehicle and tyre design. This study investigates the effect of changes in macro and micro texture on the forces generated in the contact patch. This is done by inspecting the effect of the resolution with which the surface is measured, on simulations of a vehicle driving over a rough road.

The macro texture largely affects the normal force that is created at the contact patch and influences the ride comfort. This is evaluated with the use of an FTire tyre model on a quarter car and a full-scale model respectively through simulations on a rough road. The quarter car model is used to evaluate the effects of speed, tyre model resolution and road geometry resolution on the reaction forces and moments based simulation. This analysis concludes that the speed and tyre resolution had little to no effect on the results. The road profile resolution, however resulted in a 20% error when a 15x15mm resolution was compared to a 1x1mm road resolution. A 10x10mm resolution road is ideal for a quarter car simulation. The Belgian paving, representing the rough road, was created at various resolutions on a macro texture level for full-scale vehicle simulations. This simulation data is compared to the experimental data. This experiment is solely based on evaluating the road resolution. It is found that the percentage error between the simulations and experimental data differed, depending on the resolution of the road. However, the differences were less than 5%. The simulations were compared to the most accurate road resolution and the percentage error differed by less than 10%. This indicates that a road resolution smaller than 15x15mm is only significant to highly sensitive results or quarter-car studies over a rough road when ride comfort is being evaluated.

The micro texture largely has an effect on the friction coefficient at the contact patch in the form of lateral and longitudinal force. The friction coefficient in this case is estimated with the use of a physics based model, which was validated on a flat concrete block. By comparing experimental data with the estimation data, the estimation model was found to be sufficient to estimate the friction coefficient on a rough road. The comparison resulted in a ± 6% error for the estimations. The micro texture resolution, at which the surface was measured, was subsampled to evaluate the effect it had on the estimation. It was determined that the resolution at which the micro texture is measured, influences the friction coefficient estimation. The percentage error of the estimation model changed by up to 10% for an increase of increments of 0.12x0.12mm. The change in micro texture resolution has a larger effect on the rough road than on the flat concrete road. To ensure that the percentage error stays below 10% the road should be sampled at 0.144x0.144mm for a rough road and 0.216x0.216mm for a flat road. Since the measuring

capability was limited, no conclusion can be drawn for results with a road resolution of smaller than 0.12x0.12mm.

# Acknowledgements

I would like to show my gratitude to:

- My family for always trying to understand the project and their continuous support.
- Quentin for his perfectionistic and honest editing of the report. Also his continuous love and support throughout the process.
- My fellow masters students Karthik, Gerhard, Jacques, Devin and Nico for helping to keep each other sane for the past few years, the random office conversation and the intellectual arguments.
- TK for his friendship and always being in the same boat with me.
- The VDG staff Glenn, Wietsche and Carl for the assistance of experimental work and their friendship.
- The other postgraduate students, Filip, Megan, Wian, Ross, Andries and Monique for the Oom Gert sessions and the friendship.
- Theunis for his willingness to always supply knowledgeable advice and assistance on all aspects of the project.

# Table of Contents

# List of Figures

# List of Tables

# List of symbols and abbreviations

| Abbreviations | Meaning |
|---|---|
| CNC | Computer Numerical Control |
| DFT | Discrete Fourier Transform |
| DIC | Digital Image Correlation |
| FE | Finite Element |
| GW | Greenwoods and Williams theory |
| PSD | Power spectral Density |
| RMS | Root Mean Square |
| TPD | Tyre Penetration Depth |
| WFT | Wheel Force Transducer |

| Symbols | Meaning | Units |
|---|---|---|
| $A$ | Area | $m^2$ |
| $a_T$ | Frequency shift factor | |
| $C_v$ | Heat capacity | J |
| $C(q)$ | PSD as a function of wavelength | $m^3$ |
| $D$ | Lattice constant | mm |
| $d$ | Distance between the rubber surface and pavement surface | mm |
| $E$ | Viscoelasticity | |
| $E_e$ | Elastic modulus parallel with damping | GPa |
| $E_m$ | Elastic modulus series with damping | GPa |
| $E^{''}$ | Energy loss modulus | |
| $F_1$ | Actual contact force | $m^2$ |
| $F_{adh}$ | Adhesion force | N |
| $F_o$ | Initial force | N |
| $F_x$ | Longitudinal force | N |
| $F_y$ | Lateral force | N |
| $F_z$ | Normal force | N |
| $G(q)$ | Normalized area factor | |
| $h$ | Height of road | mm |
| $L$ | Linear size of surface | Mm |
| $M_x$ | Overturning moment | N.m |
| $M_y$ | Rolling Resistance | N.m |
| $M_z$ | Aligning torque | N.m |
| N | Number of points | |
| $P_1$ | Corresponding point | |
| $P_2$ | New point | |
| $P(q)$ | Area as a function of wavelength | $m^2$ |
| $Q$ | Energy | J |
| $q$ | Wavelength | |
| $R$ | Rotational matrix | ° |
| $R_{sk}$ | Top topography | mm |
| $R_q$ | Radially averaged PSD | |

| | | |
|---|---|---|
| $R_q$ | Surface roughness | |
| $T$ | Temperature | ˚C |
| $T_0$ | Ambient temperature | ˚C |
| $\Delta T$ | Change in temperature | |
| $T_g$ | Glass transition temperature | ˚C |
| $T_{local}$ | Local rotational and translational matrix | |
| $t$ | Translational matrix | mm |
| $v$ | Velocity | m/s |
| $x_{experimental}$ | Data point that another point is being compared to | |
| $x_{simulation}$ | Data point that is being compared | |
| $z$ | Road profile height | mm |
| $z_p$ | Penetration depth | mm |
| | | |
| **Greek symbols** | **Meaning** | **Units** |
| $\zeta$ | Magnification | |
| $\eta$ | Viscosity | MPa |
| $\lambda$ | Wavelength | |
| $\mu$ | Friction coefficient | |
| $\mu_m$ | Height mean | mm |
| $\mu_{adh}$ | Adhesive friction coefficient | |
| $\mu_{hys}$ | Hysteresis friction coefficient | |
| $\nu$ | Poisons ratio | |
| $\rho$ | Density | kg/m$^3$ |
| $\sigma_v$ | Surface height variance | |
| $\sigma_0$ | Initial contact pressure | MPa |
| $\tilde{\sigma}$ | Normal stress | MPa |
| $\tau$ | Relaxation time | S |
| $\phi_z$ | Normalized distribution | |
| $\omega$ | Frequency | Hz |
| $\omega$ | Angular velocity | rad/s |

# Introduction

The forces generated between the tyre and the road at the contact patch is of importance to vehicle dynamics. All the physical interactions between the contact patch and the road are not yet fully understood. A detailed understanding of the properties involved in the contact patch can aid in many vehicle dynamics control problems, such as ABS. it can also improve current tyre and vehicle capabilities and the design thereof. The two main concepts at the contact patch is the tyre and the road itself that consists of various texture categories.

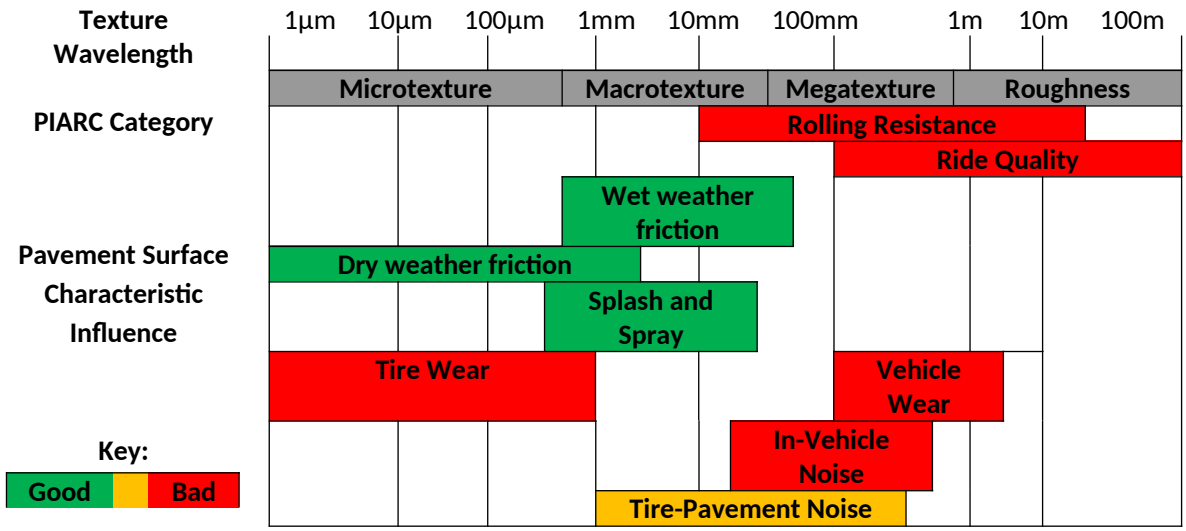


**Figure 1. Road texture compared to the effect it has on vehicle dynamics** [ CITATION Aav11 \l 7177 ]

The texture can be divided into four categories, namely the roughness, mega, macro and micro texture. Figure 1 indicates the influence that the various textures have on different vehicle dynamic properties. Wavelengths larger than 500mm determine the roughness of a surface. The mega texture comprises the range from 50 to 500mm. The roughness as well as the mega texture are usually analysed in terms of the PSD. The macro texture is considered to be in the range of 0.5 to 50mm and is more significant to the tyre-pavement noise and the ride comfort [ CITATION Aav11 \l 7177 ], where the vertical forces at the contact patch has the largest influence. The micro texture is any surface measured at a scale smaller than 0.5mm. It is determined that the micro texture has a larger influence on the friction coefficient in the form of lateral and longitudinal forces [ CITATION Ten80 \l 7177 ].

One off the essential, but often neglected components of the tyre and the road simulation interaction is the friction model. Most currently used friction models are based on stick and slip models that do not take the surface changes into consideration ([ CITATION Liu15 \l 7177 ]). For a constant flat road, this is useable; however for an off-road vehicle the stick and slip methods are no longer sufficient. The other vehicle dynamic aspect influenced by the surface texture is the ride. The accuracy and resolution required for both the terrain and the tyre for simulation purposes are debatable, especially on the road types with low frequency content, referred to as a rough road. If the simulation capability of these two aspects of the vehicle dynamics can be better understood, it could improve accuracy of vehicle dynamics simulations and thus the design of various components.

# Macro texture

As illustrated in Figure 1 and previously mentioned the macro texture of a surface largely influences the vertical forces created at the contact patch between the road and the tyre. The vertical force created at the tyre influences the ride comfort of a vehicle. The ride refers to the effectiveness of the vehicle to isolate the occupant from changes in the road to induce comfort [ CITATION Tho92 \l 7177 ]. This is not an issue on a smooth flat surface, however as the surface becomes rougher, the comfort of the passenger becomes more difficult to maintain. The ride comfort problem is investigated with vehicle dynamic simulation. The road surface used in these simulations should be a representation of the actual rough surfaces in the real world.

A significant aspect to consider when simulating vehicle dynamics is the choice of a suitable tyre model. Various mathematical models exist to attempt to model a tyre accurately. For smooth roads very basic tyre models, such as a point follower model, are used. A rough road requires a more accurate tyre model that can reflect all the tyre's properties, since the tyre flexes and deflects as it moves over various sized obstacles. The existing tyre models vary in complexity and computational time. Various tyre models are setup to either measure lateral or longitudinal, with other models are designed to simulate both. Arguably the most accurate tyre model is a fully nonlinear finite element tyre model, where the tyre is divided using a small mesh size. The FE tyre model requires extensive computational power and time. Full vehicle dynamic simulations cannot implement the FE tyre model, which limits its use. Stallmann (2013) used full vehicle dynamic simulations to compare different tyre models to determine the best tyre model for ride comfort analysis on a rough terrain. The most accurate tyre model was determined to be FTire tyre model even though it required the most input information [ CITATION Mar13 \l 7177 ].Since an FTire model is represented at a high resolution, which can be adjusted, it is assumed that the macro road texture should be measured at either a smaller or at an equivalent scale to the tyre model resolution.

The other aspect for correct simulation models is the creation of roads. For this to be possible surface should be measured at suitable resolutions, since it is significant to have a better understanding of how sensitive the tyre reaction forces in simulation (especially the vertical force for ride comfort purposes) is to the resolution at which the road profile is measured. A finer road surface can be subsampled to create a variety of roads with various resolutions, all within the macro texture range.

Quarter car models are often used to investigate ride comfort because it only has two degrees of freedom and the equation of motion is cost-effective to solve [ CITATION Tho92 \l 7177 ]. A quarter car model thus allows for the quick evaluation and investigation of specific situations and act as an estimation of how a full vehicle would react. Both a quarter car and a full vehicle model used in this study to investigate the effects of the tyre and road resolution on the ride comfort simulation results.

# Micro texture

The friction forces are the main tyre road interaction component affected by the micro texture of a surface, as seen in figure1. The lateral and longitudinal forces at the contact patch, from which the friction is determined, is caused by the rubber of the tyre that sticks and slides across the surface. The friction is largely influenced by the surface texture of the road, since it changes based on the area of the tyre that is in contact with the road. When the friction property of the tyre can be determined for the various situations and time periods, simulation of certain aspects of vehicle dynamics can be solved with more accuracy.

The FTire tyre model, used to represent the tyre in this study is known to better represent the properties of an actual tyre, since it is the only model that comprises of various aspects that is not constant as the tyre moves over a surface. These aspects includes mechanical, thermal, heat generation & transfer, tread wear, air volume, friction and flexible rim models. Whereas other tyre models only have a limited set of values for these properties. Certain properties of the tyre are significant to the friction coefficient estimation models that will be evaluated in this study. A tyre consist out of rubber and reinforcing fibers with various layers. The section of the tyre most significant to the estimation model is the tread, which comprises of rubber. Viscoelasticity, a combination of the viscosity and elasticity and the temperature effects are the most significant aspects of the rubber that is required.

The micro texture can also be measured at various resolutions and the results inspected to determine the ideal resolution by which the surface should be sampled to find the friction coefficient with relative accuracy and as little as possible processing power. The resolution is once again subsampled to determine the influence this would have on the friction value. The friction coefficient is determined with the use of a mathematical model and a practical manner to validate the model. The subsampled roads are implemented in the mathematical model to find the effect it has on the friction coefficient.

# Problem statement

The objective of this study is to determine an ideal resolution for a rough road profile for the purpose of different studies. The profile is represented in a three dimensional manner in all vehicle simulations. The effects of the resolution of macro texture scale is evaluated based on the reaction forces. The micro texture scale effects the friction coefficient. Both of these texture scales and its resolutions are evaluated.

# Chapter 1: Literature study

## 1.1 Physical models of friction

The friction coefficient between the tyre and the road is inherently difficult to measure. The methods previously used are based on empirical fits of experimental data from devices such as the British Pendulum tester [ CITATION Cal16 \l 7177 ]. Other models use physical properties and are used as estimators. These have been found to accurately estimate the friction coefficient on smooth roads. The micro texture profile of a surface affects the estimator models significantly. The friction force changes continuously over a rough road, which complicates the estimations. It was theorized that the estimator models can be used on a wide range of roads, but this has not been tested [ CITATION BNJ01 \l 7177 ]. A new method was recently developed that is derived from first principles of physics and known as either the Persson's model or the Heinrich/Kluppel model [ CITATION LiL16 \l 7177 ].

### 1.1.1 Da Vinci's model

Friction is immensely important to us, it slows down an object as it slides across a surface, especially in the case where the brakes of a car is being used. Da Vinci understood this importance and many models that followed was based on him empirical understanding of the static friction coefficient or dry friction [ CITATION Pro16 \l 7177 ]. Da Vinci set up an experiment to compare the vertical force to the horizontal force to determine the friction coefficient between any two surfaces as seen in Figure 2. This coefficient is independent of velocity and surface area.

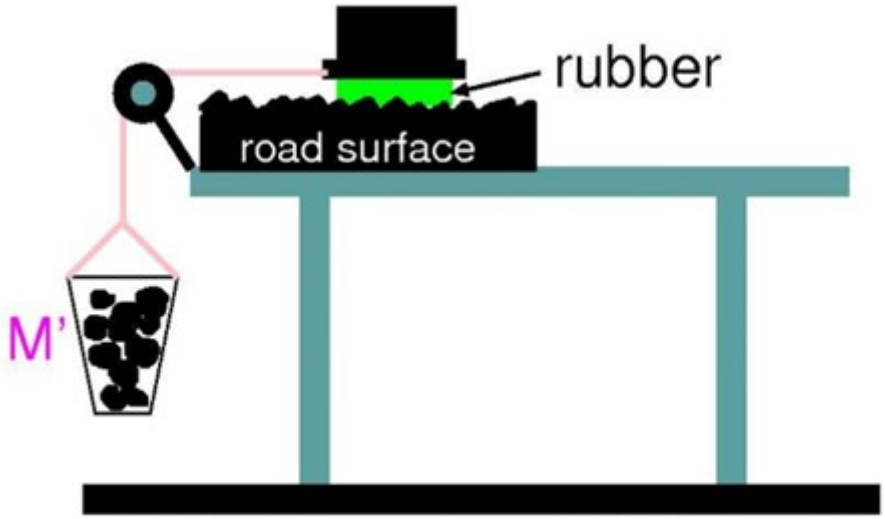


**Figure 2. Schematic of Da Vinci's friction coefficient experimental setup**[ CITATION Ame15 \l 7177 ]

### 1.1.2 Persson's model of coefficient of friction

Persson established that the friction coefficient is dependent on several physical properties and derived his model based on the following properties [ CITATION EWP14 \l 7177 ]. The friction coefficient comprises of two parts, namely adhesion ($\mu_{adh}$) and hysteresis ($\mu_{hys}$) friction. Adhesion is the rubbers tendency to cling to the surface of the road and hysteresis is the energy losses in the rubber as it deforms

and slides over the road [ CITATION Tho92 \l 7177 ]. Equations 1, 2 & 3 indicate how the adhesion and hysteresis properties can be divided into physical properties to form the friction coefficient [ CITATION EWP14 \l 7177 ].

$$\mu = \mu_{adh} + \mu_{hys} \quad (1)$$

$$\mu_{adh} = \frac{F_{adh}}{F_0} = \frac{\tau_f(v,T)A(\zeta_1)}{\sigma_0 A(\zeta_0)} \quad (2)$$

$$\mu_{hys} = \frac{1}{2}\int_{q_0}^{q_1} q^3 C(q) P(q)\, dq \int_0^{2\pi} \Im \frac{E(qv\cos\phi)}{(1-\nu^2)\sigma} \cos\phi\, d\phi \quad (3)$$

The adhesion friction coefficient is calculated by dividing the adhesion force ($F_{adh}$) through the initial force ($F_0$) that is applied before the tyre starts moving. The hysteretic friction is more complicated and determined by the PSD ($C(q)$), the normalized area of contact ($P(q)$) and the viscoelasticity ($E$ ) as functions of the wavelength and frequency.

## *Power spectral density*

The roughness of a road is specified by the Power Spectral Density (PSD) of the vertical road displacement through the use of Discrete Fourier Transform (DFT). With the use of the DFT, the road profile, in the form of height vs distance of the road, is converted into the spatial frequency domain. It should be noted that this frequency is a spatial angular frequency ($m^{-1}$) based on the length and sampling length of the road. For a randomly rough surface, the Gaussian distribution (Eq. 4) provides all the statistical properties of the surface based in the height of the topography ($h$) as a function of the length.

$$C(q) = \frac{1}{(2\pi)^2}\int h(x)h(0)e^{-iqx}d^2x \quad (4)$$

The other method through which a PSD can be created, is through a radially averaged surface roughness power spectrum, where the surface roughness ($R_q$ ) is the area under the PSD curve based on the Parseval's theorem[ CITATION Kan17 \l 7177 ]. This is once again based on the height of the road ($h$ ) and the number of points ($N$ ).

Whenever a non-random disparity occurs, such as a large valley in the road profile, it has a large effect on the PSD results. A PSD can thus be divided into two sections; a top and bottom PSD, where only the top PSD is significant for friction coefficient estimation, since the tyre will only be in contact with the top part of the road profile[ CITATION Kan17 \l 7177 ]. The top PSD is the parts that the tyre will come in contact with during the time it rolls over the surface, whereas the bottom PSD is the deeper valleys that the rubber of the tyre will never touch. By removing this 'insignificant' data of the road, a more clear picture of the actual road that comes in contact with the rubber can be seen, while still maintaining the same PSD data for the overall length. When the top PSD is calculated, a correction factor is applied where the bottom topography is replaced with zeros using Equation 5, to ensure that the PSD represents the correct statistical components of the road[ CITATION Kan17 \l 7177 ].

$$R_q^2 = \frac{1}{N_T}\sum_1^N |h_T(x)|^2 \quad (5)$$

The Gaussian distribution cannot be used to determine the PSD when a random rough surface with large differences or a small surfaces with a low long wavelength accuracy are considered. A skewed

topography is that of a road that has large valleys and these large valleys having an effect on the PSD values when only a short piece of the road is available. A different equation must be used when a so-called skew topography is being evaluated. If this occurs the appropriate portion of the road has to be selected to be stitched together to ensure that the PSD reflects the correct statistical data[ CITATION Kan17 \l 7177 ]. Two equations are used to stitch the selected data together. Equation 6 calculates the radial power spectral density based on the height of the road ($z$) and the area ($a$). This is used in Equation 7 to find the final profile of the top topography ($R_{sk}$) of the road.

$$R_q = \sqrt{\frac{1}{A}\int_A^0 \int |z(x,y)|\,dxdy} \quad (6)$$

$$R_{sk} = \frac{1}{A R_q^3}\int_A^0 \int z^3(x,y)\,dxdy \quad (7)$$

## *Viscoelasticity and flash temperature*

Viscoelasticity is a material property mostly found in rubbers, it has both viscous and elastic characteristics when it undergoes deformation [ CITATION Rod09 \l 7177 ]. This property is highly dependent on temperature, especially in rubber-like materials. An increase in temperature can be caused by the energy dissipation that occurs due to the sliding velocity between the rubber and a surface. A temperature increase will only occur if the sliding velocity exceeds $10^{-2}$ m/s [ CITATION BNJ06 \l 7177 ]. If there is no slip the viscoelastic property becomes constant and is related to the rubber properties. However, when sliding occurs, the temperature increase due to the energy loss needs to be taken into account in the form of so called 'flash temperature'. This is based on the following heat dissipation equation (Eq. 8).

$$\Delta T = \frac{Q}{\rho C_v} \quad (8)$$

From this basic heat calculation it is known that the energy ($Q$) is dissipated due to the change in temperature ($\Delta T$) caused by friction that is influenced by density ($\rho$) and heat capacity ($C_v$) of a material. The heat calculation can be represented by the viscoelasticity and thus the equation can be rewritten as Equation 9, where the actual temperature is determined by the ambient temperature ($T_0$) and other road and tyre properties:

$$T = T_0 + \frac{(q_0 h_0)^2\, ImE(\omega_0, T)}{\rho C_v} \quad (9)$$

A change in temperature of rubber causes a frequency shift horizontally along the frequency axis [ CITATION EWP14 \l 7177 ] of the results. This is depicted in the form of the viscosity loss tangent result as seen in Figure 3, which represents the ratio between the imaginary and real components of the viscoelasticity from Equation 3.

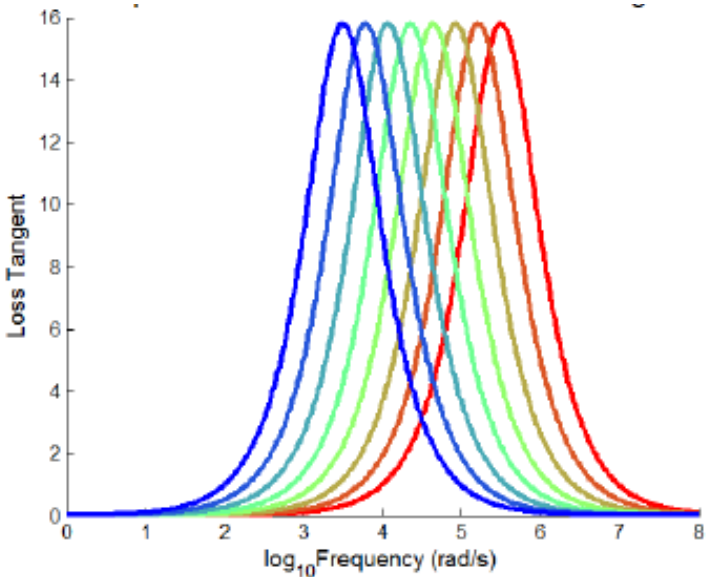


**Figure 3. Temperature effect on the viscosity loss tangent**

When the temperature increases, the loss tangent shifts to the right [ CITATION EWP14 \l 7177 ]. The William-Landel-Ferry equation is used to determine the frequency shift factor ($a_T$), that characterises the amount with which the frequency shifts.

$$\log a_T = -8.86 \frac{T - T_g - 50}{51.5 + T - T_g}$$

00

In the equation, $T$ is the local rubber temperature of the surface and $T_g$ is the glass transitional temperature, which is estimated to be 30 degree Celsius for most rubbers [ CITATION BNJ01 \l 7177 ]. The glass transitional temperature is the region in which the rubber transitions from a hard, glassy material to a soft rubbery material[ CITATION Gib15 \l 7177 ]. Even though a tyre is composed of various types of rubber and plied in different ways, it is assumed that the tread of the tyre that is in contact with the road is uniform with the same general properties. The viscoelasticity is written in terms of frequency and temperature with respect to the local rubber temperature and the ambient temperature ($T_0$) in Equation 11 [ CITATION EWP14 \l 7177 ].

$$E(\omega, T) = E\left(\frac{\omega\, a_T}{a_{T_0}}, T_0\right)$$

11

This model is not a very good description of real rubber, since the transition from the rubber region to the glassy region is very abrupt; however, the friction is found to be qualitatively correct for both before and after the transition region [ CITATION BNJ06 \l 7177 ].

## *Contact mechanics*

Persson's contact model works on the principal that if the magnification ($\zeta$) is one, the rubber is only in contact on the peaks of the road asperities, namely the macro texture. If the magnification is increased at the peak of one of these asperities, it would have more asperities on top of that with its own peaks. This will carry on until an infinite magnification in the micro texture scale. This process is shown in Figure 4. From this, it is clear that the contact patch of micro texture is complicated. The contact area is related to

the normal force and only if this force is large enough, will the rubber fill all the asperity cavities, resulting on the contact patch area being the same as the actual area of the tyre.

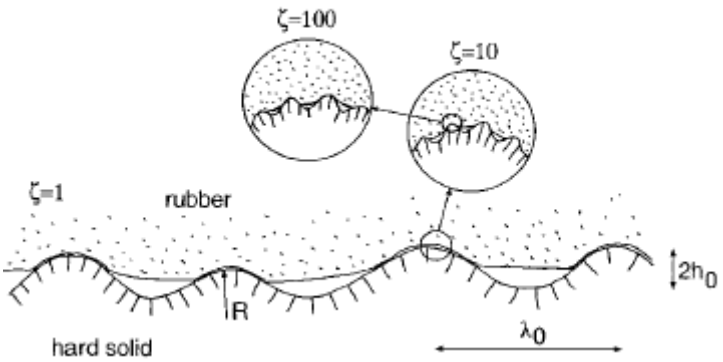


**Figure 4. Depiction of the contact of tyre with the road on various magnifications**[ CITATION BNJ01 \l 7177 ]

Equations 12 and 13 are used with the following constant for the Poisons ratio ($v$) as 0.5 to determine the area ($P(q)$) that is in contact with the road at any significant wavelength ($q$). The normalized area of contact is found from properties such as the viscoelasticity ($E$), the PSD($C(q)$), initial normal stress ($\sigma$) and the normalized area factor ($G(q)$).

$$P(q)=erf\left(\frac{1}{2\sqrt{G(q)}}\right) \quad (12)$$

$$G(q)=\frac{\pi}{4}\left(\frac{E}{(1-\nu^2)\sigma_0}\right)\int_{q_L}^{\zeta q_L} q^3 C(q)\,dq \quad (13)$$

The integrals occur over the wavelengths, where $q_L$ is the smallest relevant wavelength through $2pi/L$, where $L$ is the length of the surface. The largest wavelength is determined from $2pi/D$, where $D$ is a lattice constant [ CITATION BNJ06 \l 7177 ]. It should be noted that due to the contact mechanics model, the adhesion friction coefficient would have little to no effect on the total friction coefficient. It is also found that a Root Mean Square(RMS) roughness as small as 1um reduces the effects of the adhesion component of the friction to negligibly small [ CITATION BNJ01 \l 7177 ].

## 1.1.3 Heinrich/Klüppel model

The Heinrich/Klüppel model uses physical properties such as the elastic property at the contact patch to estimate the friction coefficient. Once again, only the hysteresis property is considered because of the RMS. The model is founded on the energy dissipated during the sliding in Equation 14. This is rearranged to solve for the friction coefficient of a rubber block undergoing deformation (Eq. 15) [ CITATION LiL16 \l 7177 ].

$$E_d=\int_0^V\int_0^T \sigma(x,z,t)\dot{\epsilon}(x,z,t)d^2x\,dt \quad (14)$$

$$\mu_h=\frac{\langle z_p\rangle}{8\pi^2\sigma_0 v}\int_{\omega_{min}}^{\omega_{max}} \omega E''(\omega)PSD(\omega)\,d\omega \quad (15)$$

The friction coefficient equation consists of the following properties: the velocity ($v$), contact pressure ($\sigma_0$), the tyre penetration depth($z_p$), the energy loss modulus ($E''$) and the PSD based on the angular frequency ($PSD(\omega)$) calculated with the use of the Fourier transform [ CITATION LiL16 \l 7177 ]. These properties are discussed in the following sections.

## *Zener slide model*

The viscoelasticity is very complex and significant property of the tyre and represented in the Heinrich/Klüppel model through the Zener slide model with Equation 16 and 17. It can be divided into two components, i.e. the rubber storage and rubber loss. With $\tau_z = \eta / E_m$ being the relaxation time of the slider and $\omega = \frac{2\pi v}{\lambda}$ the angular velocity.

$$E(\omega) = E'(\omega) + i\,E''(\omega) \tag{16}$$

$$¿\ \frac{E_e + (E_m + E_e)\omega^2\tau_z^2}{1+\omega^2\tau_z^2} + i\frac{E_m\omega\tau}{1+\omega^2\tau_z^2} \tag{17}$$

In equation 17 the elastic modulus $(E_e)$ is in parallel with the damping, represented here as viscosity $(\eta)$ and this is in series with the elastic modulus $(E_m)$ as depicted in Figure 5. Several of these models exist, however the model preferred for friction modelling is the standard linear model (Maxwell form) [ CITATION EWP14 \l 7177 ]. Typical elastic properties exist for typical tyre compounds and was found by Persson in previous experiments. These values were used as presented by Peterson, with $E_m = 10\,GPa$ and $E_e = 10\,MPa$ [ CITATION EWP14 \l 7177 ].

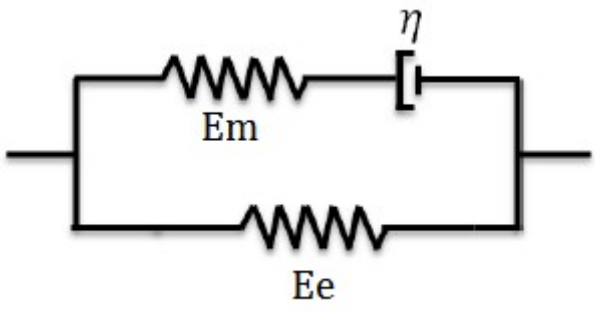


**Figure 5. Maxwell linear model for viscoelasticity[ CITATION EWP14 \l 7177 ]**

The viscosity, or rather the rubbers damping can be determined from the hysterectic damping, which is the damping caused by the friction between two planes, the one plane moves while the rubber between the two surfaces does not slip. From Figure 6 the loading and unloading cycle before slipping is depicted as a closed loop [ CITATION Rao111 \l 7177 ]. A similar loop was created from Force vs Displacement data to find the change in force ($\Delta F$) from which the damping is determined.

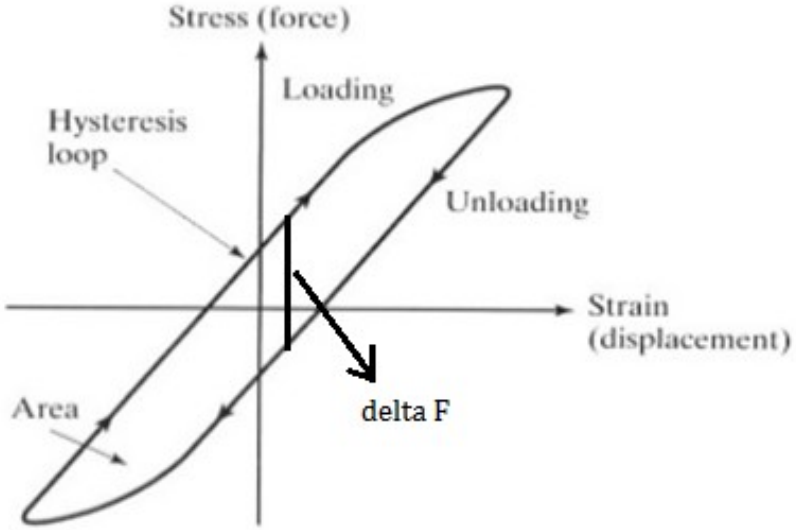


**Figure 6. Hysteretic loop** [CITATION Rao111 \l 7177 ]

## *Tire penetration depth (TPD)*

The tire penetration depth is estimated using Greenwoods and Williamson (GW) theory. The equations are based on the distance between the rubber surface and pavement surface ($d$ ), and the normalized distribution of the surface $(\phi_z)$ as seen in Figure 7 [ CITATION LiL16 \l 7177 ].

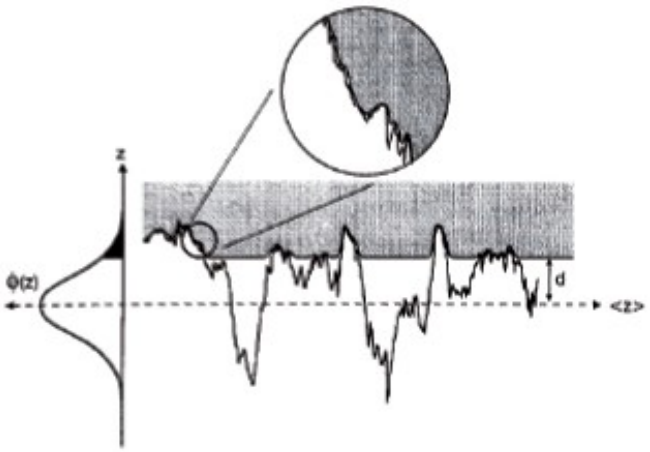


**Figure 7. Illustration of tyre penetration depth** [ CITATION LiL16 \l 7177 ]

Mathematically the TPD ($z_p$) is estimated with Equation 19, which considers the surface height variance ( $\sigma_v$), the normal stress ($\sigma$) and the adjusted force. The adjusted force takes into consideration all the effects of the tread and surface and reflects the actual longitudinal force. The tire penetration depth is dependent on multiple statistical properties of the road surface such as road profile (z), height mean ($\mu_m$) and the adjusted force determined through the use of the actual contact area of the actual force ($F_1$) of the tyre from Equation 18 [ CITATION LiL16 \l 7177 ].

$$F_1\left(\frac{d}{\sigma}\right)=\int_{\frac{d}{\sigma}}^{\infty}\left(z-\frac{d}{\sigma}\right)\frac{1}{\sigma\sqrt{2\pi}}e^{\frac{-(z-\mu_m)^2}{2\sigma^2}}dz \qquad 18$$

$$\langle z_p\rangle=\tilde{\sigma}\,F_1\left(\frac{d}{\sigma}\right) \qquad 19$$

## 1.2 Belgian paving

A rough road is needed to complete this study since both the road resolution and friction coefficient estimation needs to be calculated on a rough road. Roads are classified based on their PSD results according to ISO8608 and should fall within specific parameters to be classified as a rough road as indicated in Figure 8[ CITATION Int951 \l 7177 ]. In this graph, the road class A is considered to be a smooth road and the roughness increases as the lines move up on the PSD graph, where H is the roughest road with the highest frequencies of the vertical displacement and geometric mean.

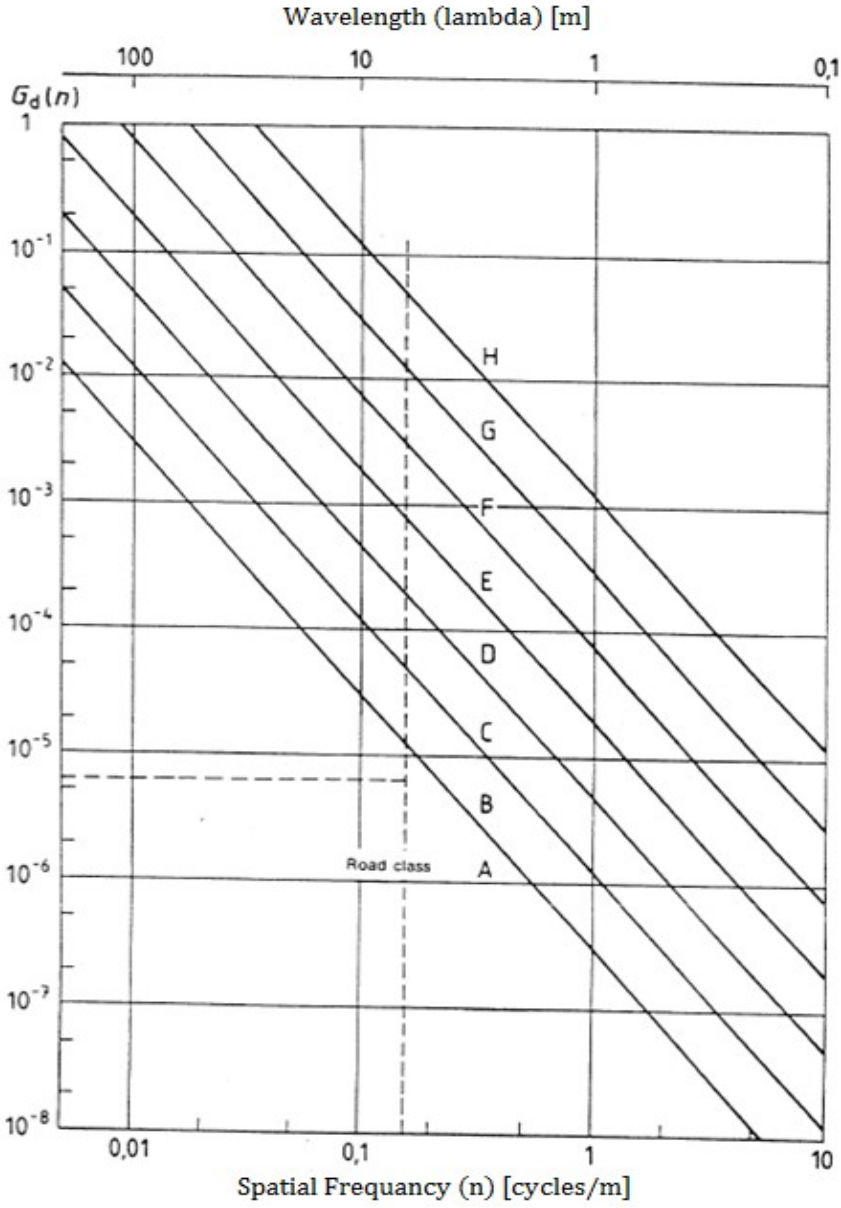


| Road class | Geometric mean [G(n)] |
|---|---|
| A | 6.3 |
| B | 25.3 |
| C | 101.1 |
| D | 404.3 |
| E | 1617.0 |
| F | 6468.1 |
| G | 25872.6 |
| H | 103490.3 |

**Figure 8. Road class classification according to PSD [ CITATION Int951 \l 7177 ]**

The represented random rough road that was available for use during experimental testing is the Belgian paving at the Gerotek Testing Facility [ CITATION Unk21 \l 7177 ] as seen in Figure 9. This is a rough road with high vertical amplitude that is attributed by a wide range of frequencies, with some discrete frequencies such as the size of the bricks.

**Figure 9. Belgian paving**

Figure 10 shows the Belgian paving PSD and a few lines indicating the various classes of road. Here it can be seen that the Belgian paving can be classified as a class D road.

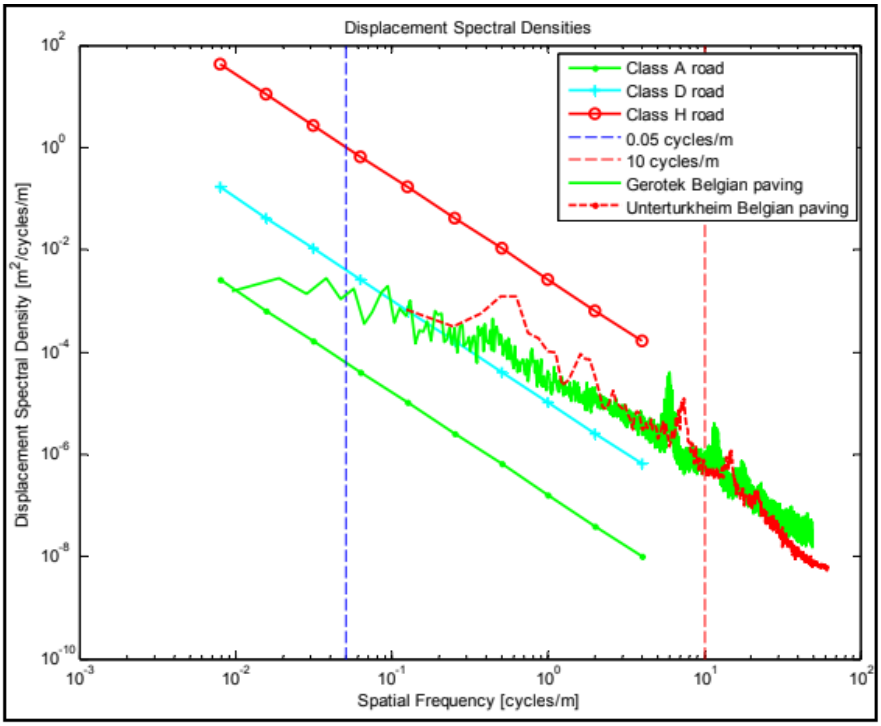


**Figure 10. Belgian paving PSD** [ CITATION Car08 \l 7177 ]

# 1.3 Surface measurement techniques

Many methods exist to measure terrain profiles. The terrain profile used in current simulations were measured with the Can-Can machine.

## 1.3.1 Can-Can

The Can-Can machine measures the rise and fall of a terrain profile mechanically. The Can-Can machine is used due to its high profiling speed, ease of data processing and low operating costs. Even though the bricks are measured to be ± 130x130mm the Can-Can machine measured it to be 164x164mm, this is due to the size of the actual hook being dragged over the road, which indicates that it 'smoothes' out the road and does not detect very sharp edges [ CITATION Car08 \l 7177 ]. This profile has been used in simulations with accurate results on different road types. However, the scale of 5x5mm rounds off any sharp edges on a rough terrain, which may be problematic [ CITATION The15 \l 7177 ].

## 1.3.2 Digital Image Correlation (DIC)

Digital image correlation is one of the more complex methods used to measure the road profiles, where previously the Can-Can method simplified the measurement [ CITATION Car08 \l 7177 ]. Stereo vision works with two images taken simultaneously of the same scene, which in this case is the road and stitches them together to form a 3D image of the entire road. This is then converted into data points to represent the road profile.

### *Calibration*

Calibration is necessary to find the relative position, orientation and relationship of the view of the two cameras that is used during post processing. Stereographic vision was used in this instance, which is when two cameras each take an image from a fixed position relative to each other of the same scene.

Stereography works on the same principle as that of the human eye when it determines the depth of what sees based on the distance between two objects. The further the scene is from the camera, the

smaller the distance is between the same point on the two images. When the scene is closer to the cameras, the distance becomes larger and from this the depth is estimated [ CITATION The15 \l 7177 ]. Multiple images are taken of an asymmetrical calibration sheet, with pre-known distance between the circles, at slightly different angles to find an averaged calibration. A least squares approach is used to calculate the relative orientation between the cameras.

### *Road profile creation*

Digital image correlation is often used to measure as small as a micrometre resolution of a surface because of the easy implementation and non-contact approach, this is however dependant on the type of camera being used. The relative motion between sequential images can be determined by tracking identifiable points on the image. To track the changes between two consecutive images, easily identifiable points, known as features must exist in these images such as changes in the texture or colour [ CITATION The15 \l 7177 ]. These features are then tracked across the images even when the images are not obtained from the same orientation, allowing for some leniency.

The resolution of the cameras (Appendix A) used in the stereo vision rigs can be set to a minimum of 640x480. On average, the image pair results in 400x400 3D points that in turn results in a 1x1mm resolution road. This can easily be sub sampled to create different macro texture roads with various resolutions. Every single image pair taken with the stereo vision rig creates a 3D image of a section of the road that is then joined and overlapped with a process referred to as registration. This results in various 3D points which has undergone rotation and translation from one 3D image to the next [ CITATION The15 \l 7177 ]. Once the 2D points (in the x-axis and the y-axis) relative change in motion has been tracked between two images, the change in height (z-axis) can also be found. This is done with the use of a rotation matrix $(R)$and a translational vector$(t)$. Where $P_1$is the correspondence point and $P_2$is the new point and is used as the new correspondence point in the third image with Equation 20.

$$P_2 = R\,P_1 + t \tag{20}$$

$P_2$ is only calculated between two images and should thus be expanded into a matrix form to take into account a whole set of images, as in Equation 21. Within the $T_{local}$ matrix the rotation and translation is tracked from image one to image two, relative to image one.

$$T_{local} = \begin{bmatrix} R_{11} & R_{12} R_{13} & t_x \\ R_{21} & R_{22} R_{23} & t_y \\ R_{31} & R_{32} R_{33} & t_z \\ 0 & 0 \quad 0 & 1 \end{bmatrix} \tag{21}$$

The matrix allows for the translational and rotational tracking between two images to create a global position and orientation of the surface. With the registration method, the 3D cloud surfaces will overlap with 50%. The inverse distance method is used to interpolate these clouds to find the final point, which serves as the average over all the point cloud surfaces [ CITATION The15 \l 7177 ]. This ensures that even after the images have been overlapped, the sampling points occur at a constant frequency. The DIC method was used in this study to measure road profile at a finer resolution than that of the Can-Can machine.

## 1.4 FTire

The FTire model comprises of a flexible ring model, with multiple layers with multiple body belts. The flexible ring flexes and extends radially, tangentially and laterally as seen in Figure 11. This assists in the simulation of how a tyre's different layers responded to the tyre/road excitation.

**Figure 11. Schematic of how the flexible rings can rotate** [ CITATION Gip141 \l 7177 ]

The manner in which the tyre model deflects is made possible by ring segments being attached to each other with nonlinear springs and dampers as illustrated in Figure 12. These characteristics are determined through extensive experimental testing. Input data to create the model consisted of various physical properties, parameters and test data. The more known properties added to the model, the least estimations need to be made, which increases accuracy of the model [ CITATION Mar13 \l 7177 ].

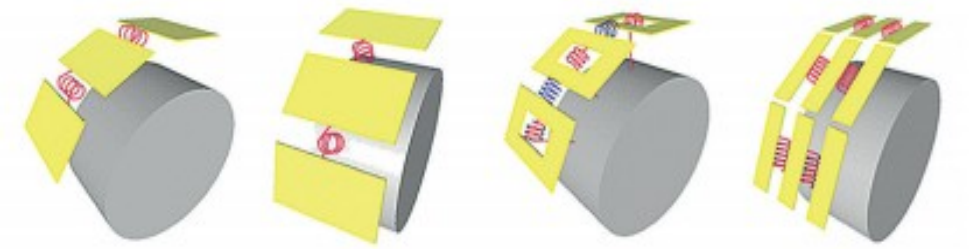

**Figure 12. An example how the stiffness and deflection acts in all the different directions** [ CITATION Gip141 \l 7177 ]

When an FTire model is being created, many properties can either be set to one standard value or it can have a separate model. For example, the tyre pressure can be kept constant or a model can be created to represent changes in pressure either at certain time periods or specific situations. This enables various fluctuating aspects and flexible use of the model.

Since high resolution tyres models exist, the road needs to be measured at an equivalent scale. The optimum road resolution needs to be determined, to find the correct scale of accuracy. Cosin, the creator of the FTire model warned that there is a percentage error difference when the results from various road resolutions are compared to each other, as seen in Figure 13 [ CITATION Gip141 \l 7177 ]. Significant percentage error differences exist for the reaction forces of a tyre rolling over a road.

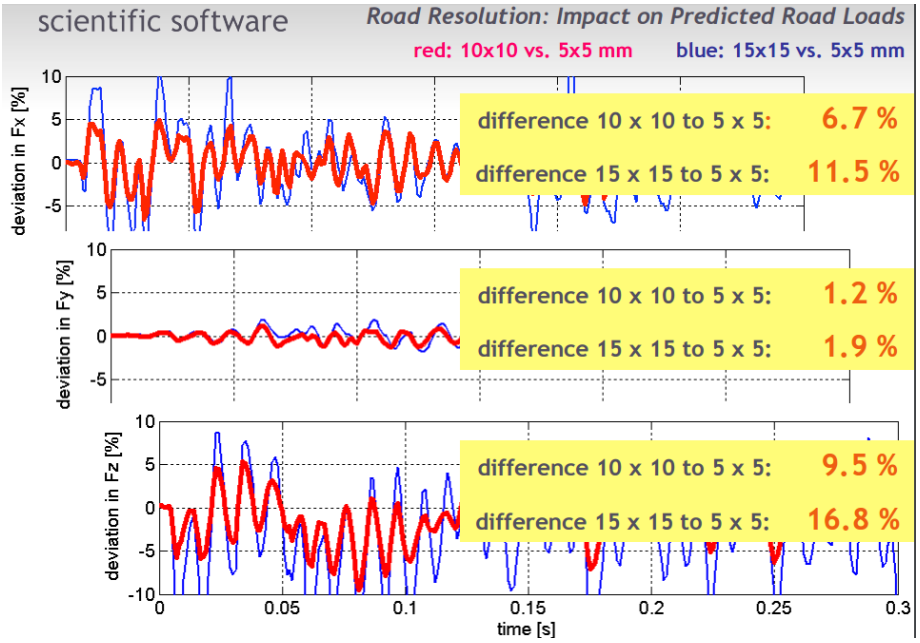


**Figure 13. Percentage difference of various road resolutions (Gipser & Hofmann, 2014)**

## 1.5 Percentage error

The percentage error is calculated with Equation 22. The percentage error is used to determine the averaged accuracy when two sets of data are compared to each other. Equation 22 is used as indicated where the $x_{simulation}$ is the data point compared relative to the data point of the $x_{experimental}\_\mathrm{data}$ to determine how close the simulation data is to the experimental data. The values for the experimental or simulation points could be used to compare any two sets of data to each other.

$$percentage\,error = \sqrt{\frac{\sum \left(x_{experimental} - x_{simulation}\right)^2}{\sum \left(x_{experimental}\right)^2}} \times 100 \qquad 22$$

# Chapter 2: Macro texture

This section evaluates the effect of the macro texture road profile resolution on the forces and moments created at the contact patch. A thorough study was done by sub-sampling the Belgian paving, measured using DIC, to various resolutions. A quarter car model was first evaluated using simulation results and then a full scale model was compared to experimental results.

DIC was used to measure a 5m long section of the Belgian paving at a 1x1mm resolution, which was then subsampled to represent other resolutions. A 3D road profile was created for the use of the quarter car simulations. A sample of the Belgian paving is shown in Figure 14 to indicate how the different resolution sizes compare to each other. The two resolutions are overlaid.

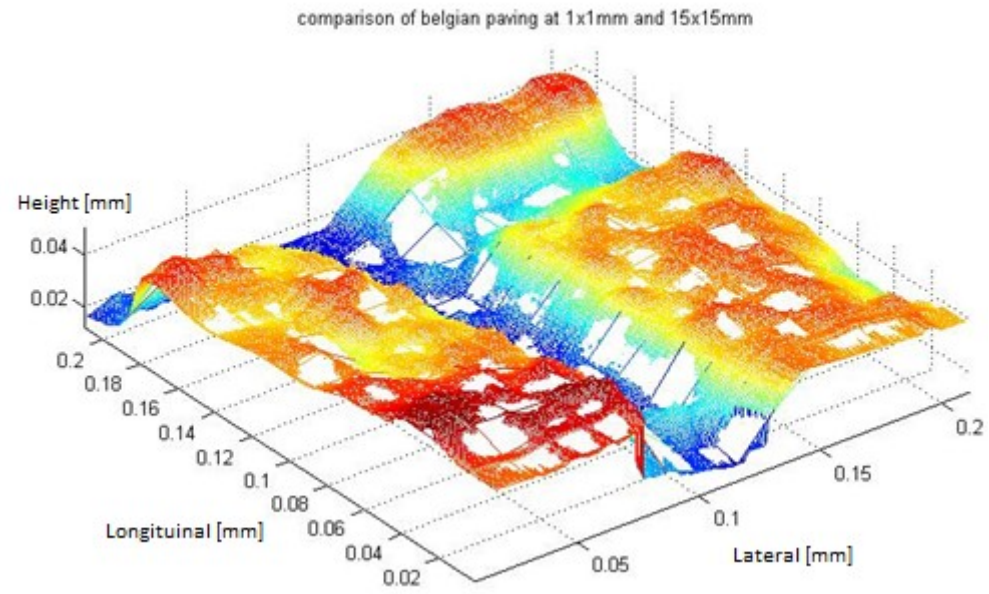


**Figure 14. Resolution of road model**

The full-scale vehicle simulations were performed over a different section of the Belgian paving. The measured road profile was processed into a three dimensional road in a matrix form with x, y and z-coordinates similar to Figure 14, with the use of DIC. Where the x and y represents the width and length of the road and z the height. The full length of the Belgian paving at Gerotek is 100m, however it was assumed that a smaller portion of the road would result in the same outcomes required to evaluate the contact patch. This was why only 1m section of the Belgian paving was used. For this to be possible, a mold was made from the Belgian paving of the required section out of a polyurethane compound, through DIC the mold was compared to the actual paving with a less than 10% error. Concrete was poured into this mold to make a positive of the paving and ramps built on either side of the block with a low angle (<10°) a depicted inFigure 15. A section of a rough road is measured at 1x1mm resolution, which is considered to represent the macro texture scale. It should be noted that the on and off-ramp profile could not be created through DIC since it was a very smooth surface with very little definition. It was thus created manually. This created a smooth ramp and could cause discrepancies in the simulation. It was previously determined that the sub-sampled roads represent the same profile as that of the road, however it was seen that the smaller resolution showed more detail than the larger resolutions in Figure14 where the smaller and larger resolutions are over laid.

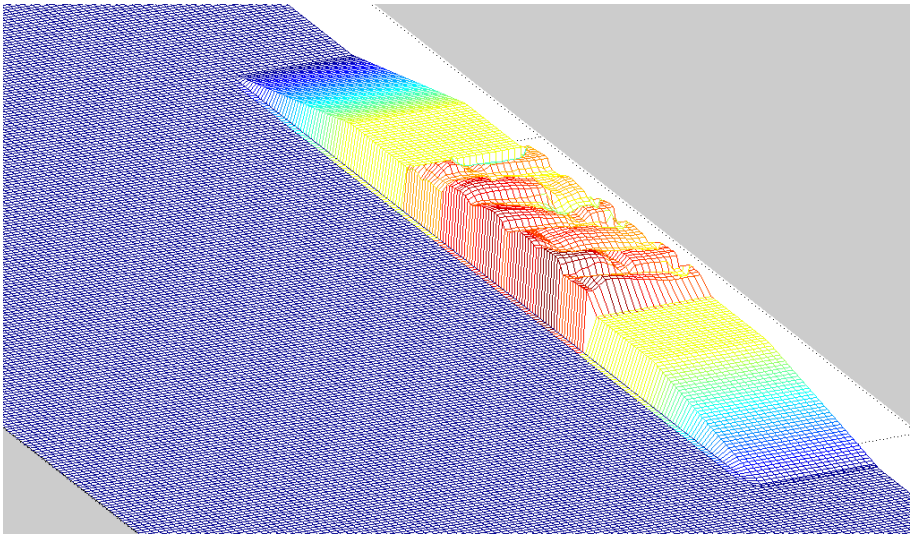

**Figure 15. Model of the Belgian paving ramp**

The Belgian paving is considered as a skewed topography, as mentioned in the literature study. To create the correct PSD profile of this rough road, the appropriate part of the top topography was selected to be stitched together. Since there were extremely large valleys throughout the Belgian paving a section on the top part of one of the paving blocks were selected to represent the PSD as seen in Figure 16.

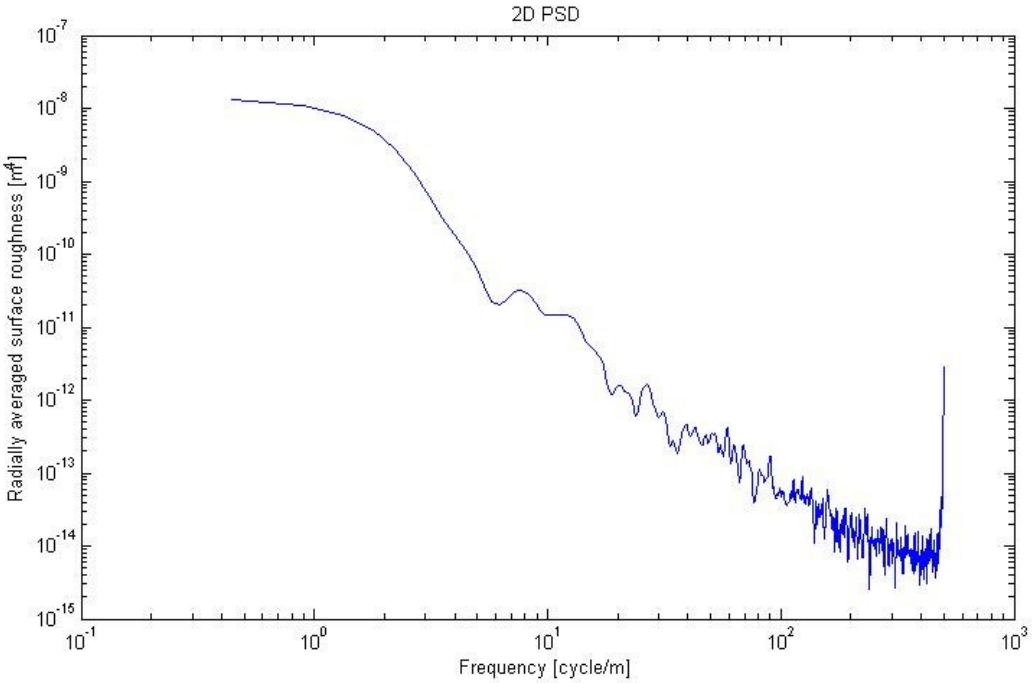


**Figure 16. Top PSD for Belgian paving**

# 2.1 Quarter car model

## 2.1.1 Simulation

The Adams quarter car model was based on the properties of the full scale vehicle. Thus, the quarter car model (Error: Reference source not foundError: Reference source not found) represents an actual quarter of the full-scale model. The tyre used throughout the experimental tests, driven over the Belgian paving bump and the tyre tread in the friction estimation tests is a Michelin LTX/AT2. The specifications for this tyre is shown in Table 1 [CITATION Mic18 \l 7177 ]. A Michelin FTire tyre model was imported into Adams to represent the various elements as seen in the literature study [ CITATION Bos16 \l 7177 ]. These elements were then adjusted to evaluate the effect that the tyre resolution would have on the results. The quarter car model was driven over the section of Belgian paving at various speeds, with different resolutions.

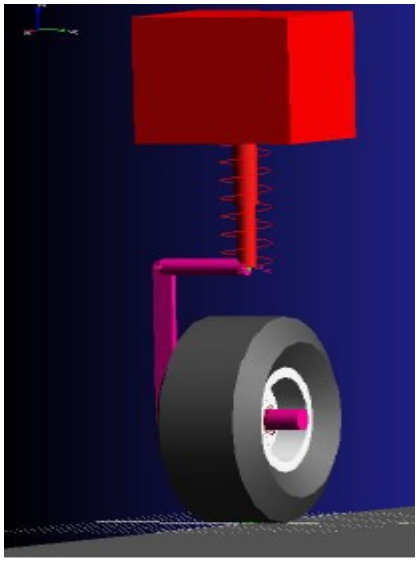

Figure 17. Quarter car CAD model

Table 1. Michelin LTX/AT2 tyre specifications

| Specification | Specification value |
|---|---|
| Size | LT245/75R16/E |
| Service Description | 120/116R |
| Sidewall | ORWL |
| MSPN | 33367 |
| Rim Width Range [inch] | 6.5-8.0 |
| Section width on rim width | 9.76 on 7.0 |
| Overall diameter | 30.47 |
| Tread depth [in/32nds] | 17 |
| Revs/Mile at 45 mph | 683 |
| Max Load single [lbs@psi] | 3042@80 |
| Max Load dual [lbs@psi] | 27778@80 |

## 2.1.2 Effects of speed

The simulations were performed at various speeds (5km/h, 10km/h, 15km/h & 60km/h) to investigate how it would affect the forces and moments at a road resolution of 1x1mm (Figure 18(top)) and 15x15mm (Figure 18(bottom)). It is clear from the results, that as the speed increased, so did the amplitude of the data. The same trend was seen for the forces and moments in the other axes. When the speed increased, it had little to no effect on the percentage error when the two road resolutions data were compared to each other. The percentage error differed by less than 5%, which is negligibly small. It was found that the 60km/h data was of a large magnitude and deemed unreliable. This was caused by the quarter car model becoming unstable at speeds higher than 40km/h, since the loss of contact occurs between the tyre and the road [ CITATION Sie10 \l 7177 ].

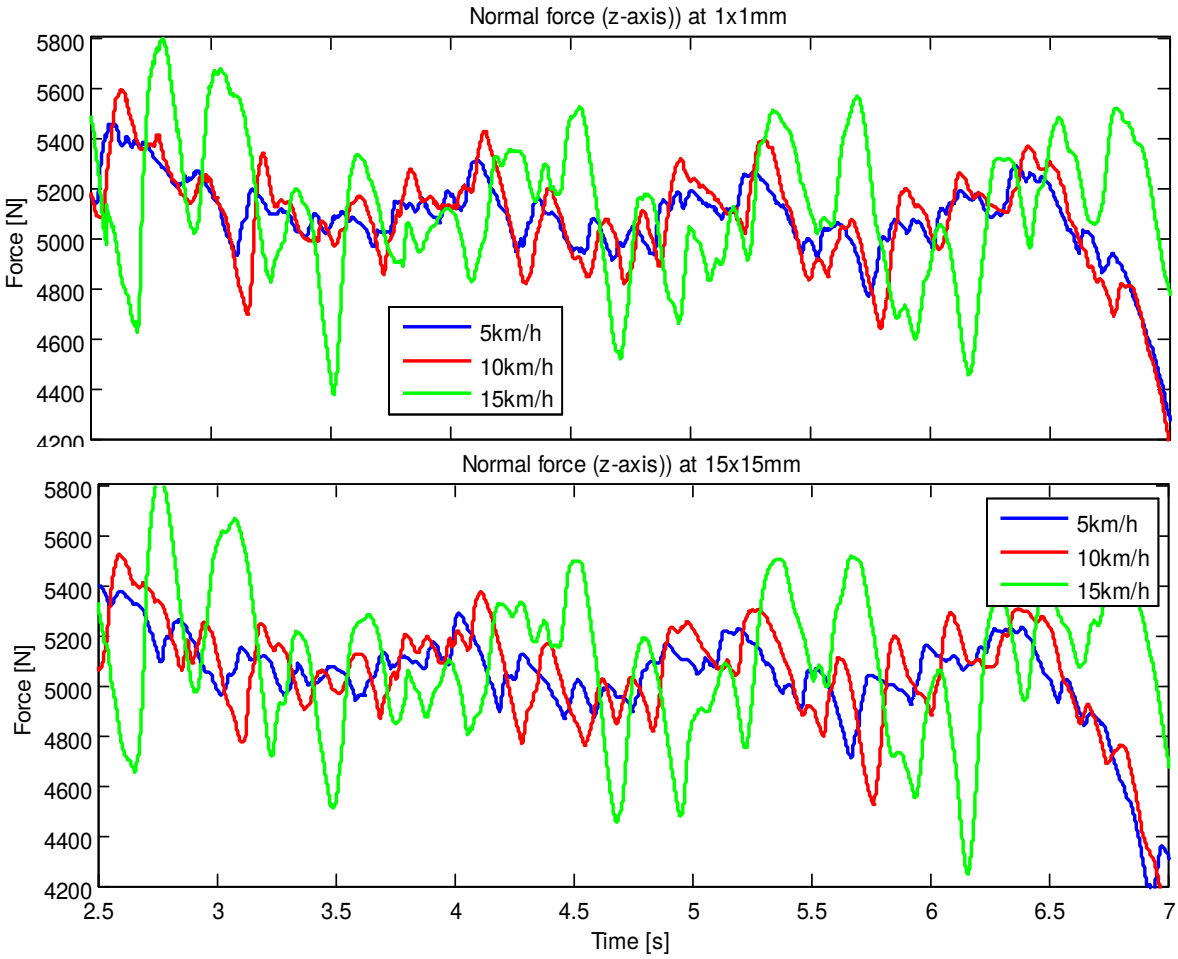


**Figure 18. The normal force results at various speeds for the 1x1mm (top) and 15x15mm (bottom) road resolution**

## 2.1.3 Tyre resolution effects

Since the study was done based on the resolution of the road and the effect it has the tyre reaction forces, it was also important to investigate the effects that the resolution of the FTire model has on the results. The tyre model resolution could provide insight into the computational time and possible increase in percentage error.

The tyre resolution was determined by the various factors. The belt segments that are set up in all directions as was shown in the literature study. The contact points per belt segment, which defines the points where forces are detected on the contact patch. And the number of strips into which the contact elements are arranged proportional to the contact elements. All these factors have a limit after which the resolution can be made even smaller, but it will have insignificant effects on any of the data, as stated by the Cosin reports [ CITATION Gip141 \l 7177 ]. The standard and most commonly used tyre resolutions, as recommended by Cosin software, is with the belt segments set to 80, contact elements to 40 and the number of strips to 20.

Due to these limits, it was decided to evaluate double and half of the current resolutions of the tyre, which is the same as the recommended amounts. It was found that when the higher limits were exceeded, the simulation tended to fail since there were too many elements to solve for. If the lower limits are exceeded the tyre model becomes unstable and also fails. It was determined that a change in tyre resolution had little to no effect on simulation results as seen in Table 2. With the percentage error, determined from Equation 22, below 4% of the forces and even smaller effects on the moments. It should

be noted that this only takes into account a straight driving situation; this might look different for cornering and braking situations.

**Table 2. Percentage error of the various road resolutions with change in tyre resolutions**

| | Tyre resolution | 1x1mm | 15x15mm |
|---|---|---|---|
| **Fx** | Double | 1 | 1 |
| | Half | 4 | 2 |
| **Fy** | Double | 1 | 1 |
| | Half | 2 | 3 |
| **Fz** | Double | 1 | 1 |
| | Half | 2 | 2 |

### 2.1.4 Road resolution

It was assumed that the 1x1mm road resolution was the most accurate representation of the data and thus the larger road resolutions were compared to this, with use of the percentage error equation. These simulations were done at 5km/h, since it was already determined that the speed had little to no effect on the results. The results of these simulations are seen in Table 3.

**Table 3. Percentage error of forces and moments based on change of 5x5mm resolution**

| Road resolution | 5x5mm | 10x10mm | 15x15mm |
|---|---|---|---|
| **Fx** | 7 | 9 | 10 |
| **Fy** | 8 | 14 | 16 |
| **Fz** | 5 | 15 | 22 |
| **Mx** | 5 | 7 | 9 |
| **My** | 3 | 4 | 6 |
| **Mz** | 5 | 6 | 8 |

Table 2 indicates that the normal force was influenced the most by the change in road resolution, with the lateral force a close second. While the overturning moment was affected the least. It was significant to note that the percentage error increased as the resolution increased, with the largest error at ±22%. It was not possible to determine a good average from this data since the results varied in the different axes. The percentage difference is the largest for the normal force with almost ±20%. The lateral and longitudinal forces percentage errors start off the same, however, the lateral force increases with larger increments (± 8%). The moments are more constant with increments of ±2% between the road resolutions.

## 2.2 Full-scale model

The road resolution was now investigated on a trailer that represents a full-scale vehicle model, which can take into account the roll of the body and considered a more stable model than a quarter car model, especially at higher speeds.

### 2.2.1 Experimental work

The experimental work was done on a test trailer as seen in Figure 19 and the simulations done on an Adams model Figure 19 (top). Various tests were done to determine the physical properties of the trailer to be able to build an accurate model. The trailer hitch was modelled to be able to rotate as and actual hitch of a trailer would when connected to a vehicle. The trailer was driven over bumps in various manners, with only the right wheel, only the left wheel and then both wheels to compare the simulation

to the experimental data to validate the model. The response of the trailer through the excitation forces and tyres of the simulation data correlated with the experimental data [ CITATION Zur17 \l 7177 ].

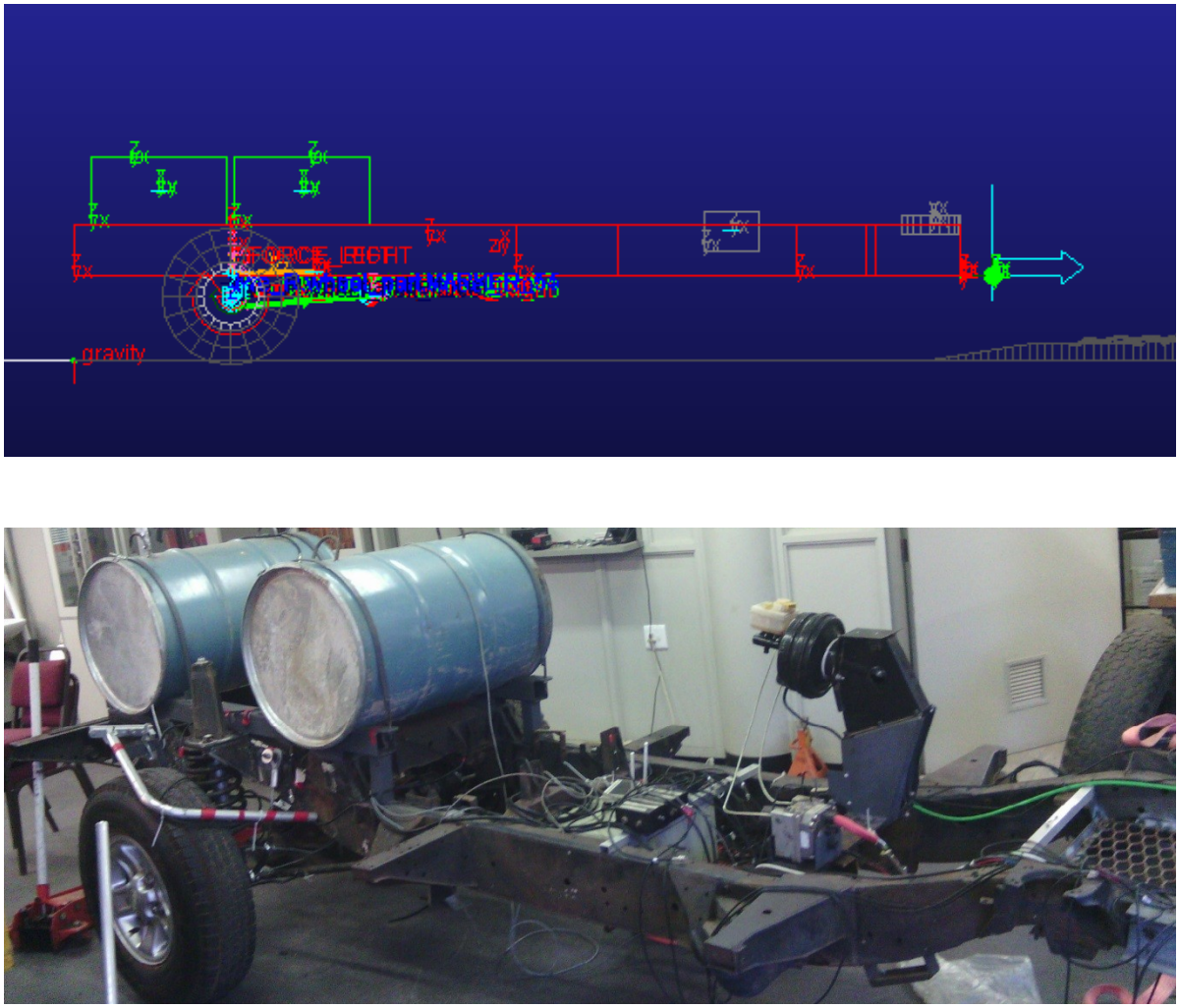


**Figure 19. The trailer during experimental work (bottom) and simulations (top)**

To measure the forces and moments in the wheel, a Wheel Force Transducer was attached to both wheels[ CITATION Els12 \l 7177 ]. The wheel force transducer (WFT) is used to measure the forces and moments on all three axes systems on the wheel hub, this is achieved through having two rings, one attached to the rim and the other to the hub. These two rings are connected to one-another by six load cells. It forms a part of the hub to ensure that all the forces and moments act through it during driving conditions as seen in Figure 20. Wheel rotation angle is also measured to determine the related forces and moments. As the WFT turns with the wheel, a daq system is attached to track the rotation of the wheel and stores the data. Data is post-processed to get the resultant forces, moments and wheel rotation angle.


**Figure 20. WFT during testing** [ CITATION Els12 \l 7177 ]

Two cameras were attached to the trailer to measure the road profile directly behind the tyre to ensure that the track over which the tyre travelled was used to create a road profile through the use of DIC. The trailer was driven with one wheel over the Belgian paving and one wheel over the smooth road to isolate the measurements. The trailer was hitched to a vehicle and the trailer was dragged over the Belgian paving bump at 5km/h. It was decided to run all the experiments at 5km/h since it was determined from the quarter car evaluation that the speed had negligible effects on the results in the forces and moments. A low speed was also chosen because it would result in more stable low frequency forces and moments.

## 2.2.2 Simulation

The simulations where performed at the same constant speed at which the experiment was performed (5km/h) to be able to compare the data. With the trailer model running with one wheel over the DIC created ramp profile and one wheel on flat road. The sampling frequency during simulations were done at 2KHz, the same as the sampling frequency during experiments to prevent aliasing on the rough road.

## 2.2.3 Discussion of results

The experimental and simulation data of the forces and moments in the various axes are discussed in this section.

### *Longitudinal force (Fx)*

The results are indicated in Figure 21, where it is also made clear where the Belgian paving, on and off ramps were relative to the data. The same detail is seen for both the experimental and the simulation data; however, there is a notable amplitude difference, especially on the Belgian section. The 1x1mm and 5x5mm resolution of the road show the same results. The 10x10mm road indicates the best comparison with the experimental data, while the 15x15m road had the worst percentage error difference. It can also be seen that the results for all the various road resolutions are close to each other.

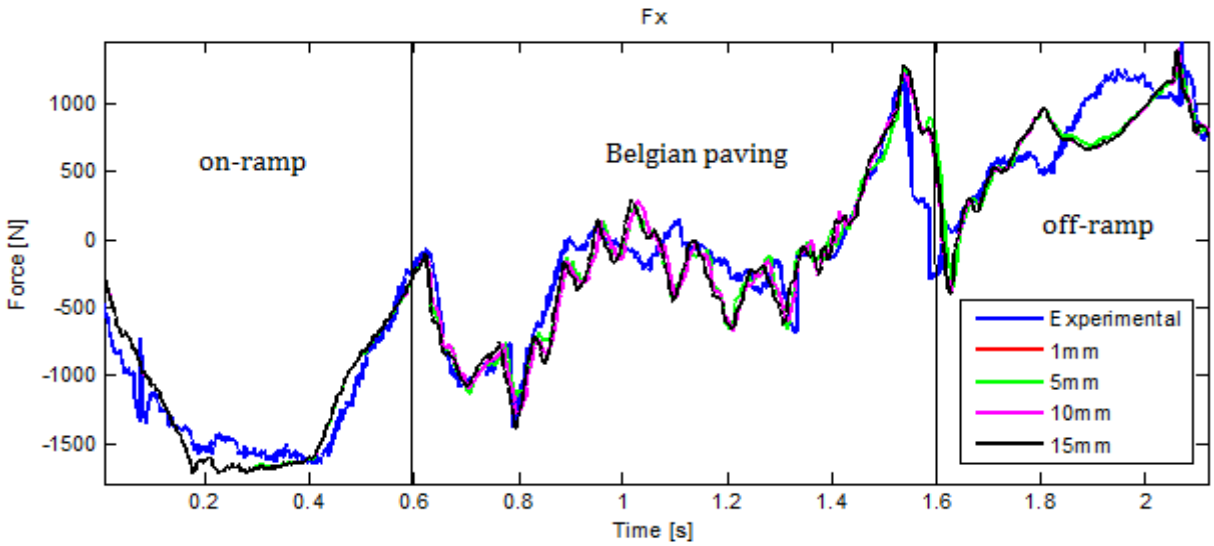


**Figure 21. Longitudinal force of the simulation and experimental data**

## *Lateral force (Fy)*

The general trend of the lateral force results looks good, however on the on- and off-ramp the shape of the graph does not reflect the same as the experimental data, as seen in Figure 22. This is can be attributed to the manner in which the smooth ramps were modeled. The friction coefficient change from the Belgian paving to the ramp plate causes the larger change in lateral force from the ramps to the Belgian paving. As for the longitudinal force, the 1x1mm and 5x5mm resolution results are similar in nature. Interesting enough the 15x15mm resolution was the closest to the experimental data, and the 1x1mm the furthest from it. Once again, the simulation results compared well for the various road resolutions.

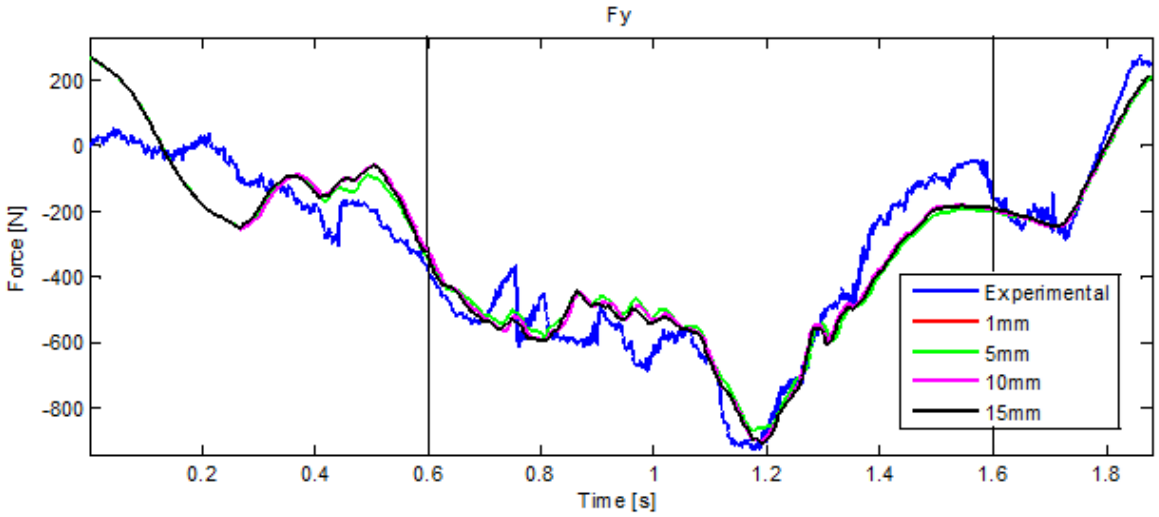


**Figure 22. Lateral force of simulation and experimental data**

## *Normal force (Fz)*

The general trend of the simulation data was good (Figure 23), however the on and off ramp's shows very little detail in simulation, once again caused by the modeling of the ramps. There were no changes between the simulation data of the 1x1mm and the 5x5mm resolution roads and very small percentage error between any of the data from the various road resolutions.

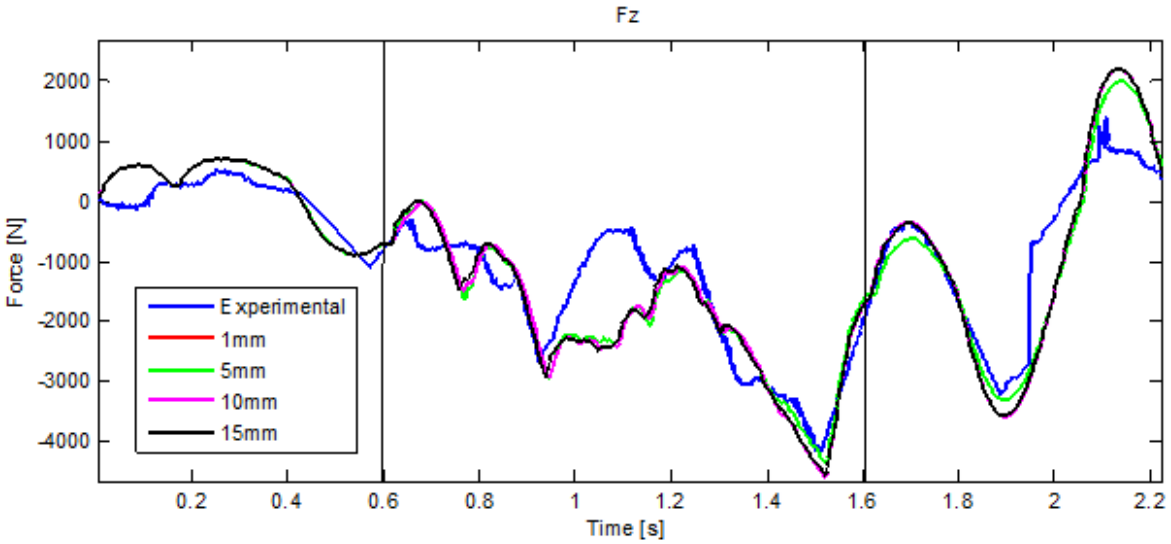


**Figure 23. Normal force of simulation and experimental data**

## *Overturning moment (Mx)*

The same general trend seen in the results of the forces could be seen for the moment about the x-axis when experimental data was compared to the simulations (Figure 24). The small amount of detail on the ramps are again noticed. It was significant to note that the moment about the x-axis is the least dependent on the resolution of the road. This can be seen from how closely the various resolution results are to each other.

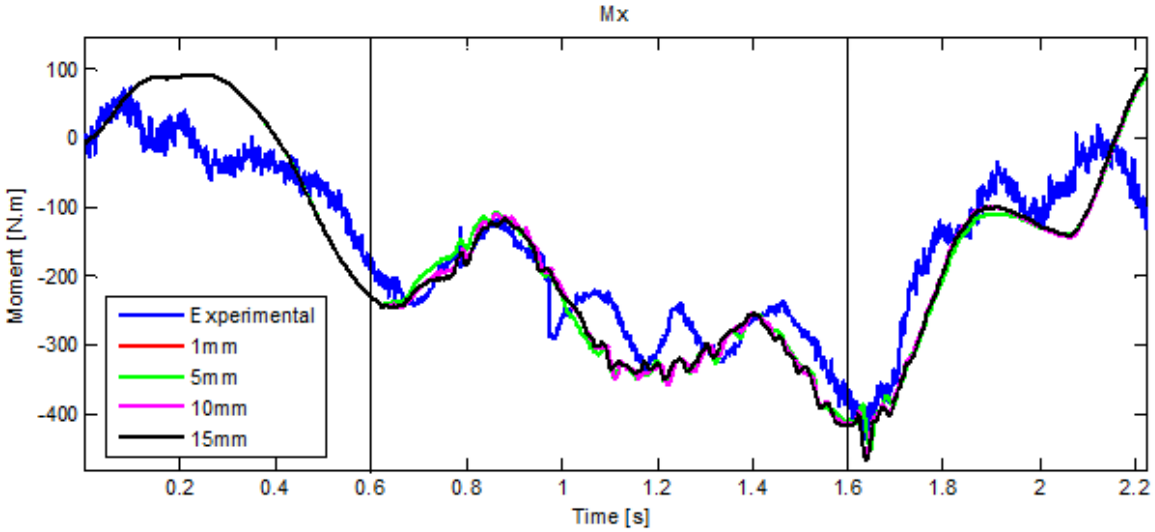


**Figure 24. Overturning moment of simulation and experimental data**

## *Rolling resistance (My)*

As expected, the moment about the y-axis showed the smallest reaction moment values with results of the experimental data close to zero, as seen in Figure 25. The simulation data has a much larger amplitude and magnitude when compared to the experimental data; this was caused by a random excitation frequency in the simulation caused by vibrations in the trailer. Both sets of data are of small value when compared to the other moments in the other axes, with smaller values of the simulation data.

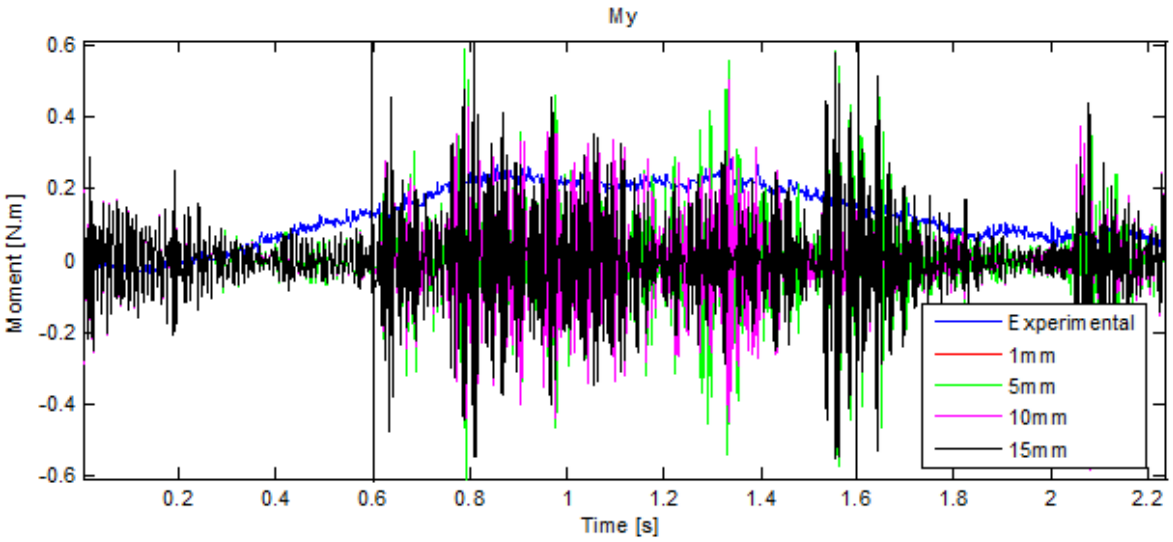


**Figure 25. Rolling resistance of the simulation and experimental data**

## *Aligning torque (Mz)*

The simulation data followed the same general trend as that the experimental data. This is the only set of results where the 1x1mm percentage error is not the same as the 5x5mm (Figure 26). This indicates that the moment about the z-axis was the most sensitive to the change in road resolution.

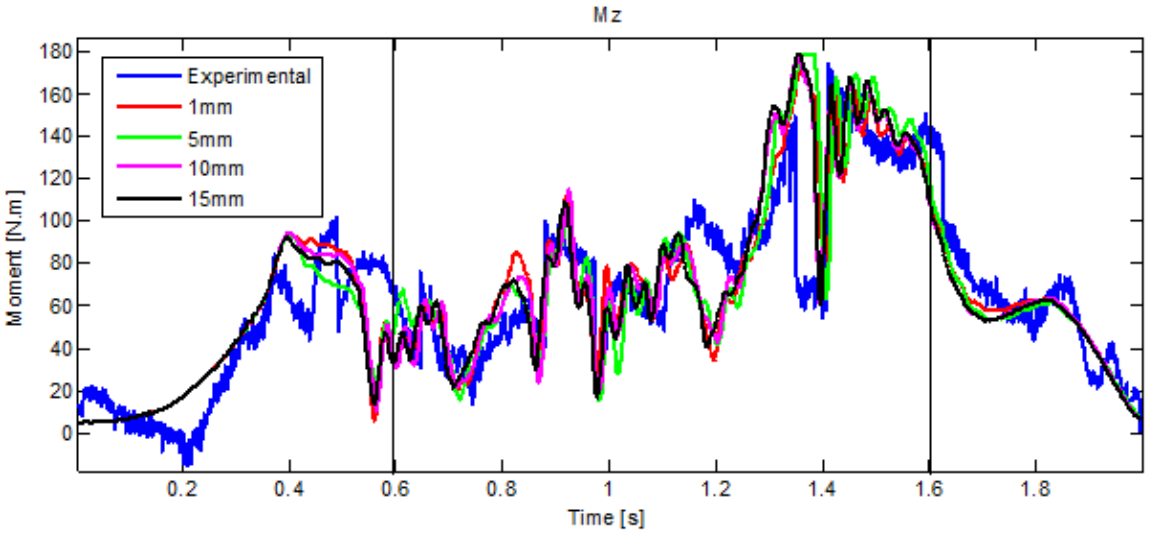


**Figure 26. Aligning torque of the simulation and experimental data**

## 2.2.4 Percentage error simulation vs experimental

The percentage error is used to determine the averaged accuracy when two sets of data are compared to each other. Equation 22 is used to find the percentage error. The three forces and three moments were compared separately to the corresponding experimental data with the use of the percentage error calculations. The results are summarized in Table 4.

Table 4. Percentage error for the simulation with various road resolutions compared to the experimental data

| Road resolution | 1x1mm | 5x5mm | 10x10mm | 15x15mm |
|---|---|---|---|---|
| **Fx** | 26 | 26 | 26 | 26 |
| **Fy** | 25 | 25 | 24 | 24 |
| **Fz** | 39 | 39 | 41 | 41 |
| **Mx** | 30 | 30 | 30 | 30 |
| **My** | 10 | 10 | 12 | 12 |
| **Mz** | 31 | 32 | 30 | 31 |

The trend of simulation compared to the experimental data of the longitudinal force was good based on the accuracy of the simulation (± 26%), with a very small difference between the various resolutions. This number can be decreased if the on and off ramp are modelled with more accuracy. When only the Belgian paving section was evaluated, the percentage error decreased to 18%. The difference between the most and least accurate results were less than 2% for the normal force, thus indicating that all the different resolution roads were equally accurate. The normal force's percentage error followed an expected trend, where the 1x1mm resolution was the most accurate and the percentage error increased as the road resolution increased. Once again the changes between the accuracies were less than 2%. The different resolutions had a small effect between it and the experimental data or the overturning moment, with less than 0.5%. The percentage error was also the smallest with ±15% for the rolling resistance. The 1x1mm resolution was the most accurate; however, the difference between the errors from 15x15mm to 1x1mm road resolution was only ±1%. The aligning torque had the largest percentage error, nevertheless the percentage error varied with small amounts.

### 2.2.5 Percentage error simulation vs simulation

The simulation results for various road resolution was now compared to the 1x1mm road resolution. The 1x1mm resolution was chosen since there was little error difference in table between the various road resolutions. This was done to determine if Cosin's warning that a difference exists when the results of various road resolutions, when they are compared to each other [ CITATION Gip141 \l 7177 ], as seen in section 1.4. To determine if this was only possibly true when the simulation results were compared to each other. A summary of the percentage error results for simulation compared to simulation can be seen in Table 5.

Table 5. Summary of simulation data compared to the 1mm road resolution

| Road resolution | 5x5mm | 10x10mm | 15x15mm |
|---|---|---|---|
| **Fx** | 0 | 6 | 8 |
| **Fy** | 0 | 4 | 4 |
| **Fz** | 0 | 7 | 8 |
| **Mx** | 0 | 4 | 4 |
| **My** | 0 | 3 | 3 |
| **Mz** | 11 | 12 | 12 |

Since 1x1mm and 5x5mm road resolutions had exactly the same results for most of the forces and moments the percentage error was zero for the 5x5mm road resolution. The aligning torque was the only exception, which had a 11.31% percentage error. The percentage error for the forces in all three axes were small and below 8%, with a larger percentage error for the longitudinal and normal forces. This was however considered to be small enough to be negligible in simulation results. The moments were rather

different with a percentage error under 12.3% and once again indicating the aligning torque was the most sensitive to the change in resolution with the highest percentage error.

## 2.3 Conclusion

From the quarter car simulations, it can be concluded, that the change in speed before it becomes unstable, has negligible effects on the resultant forces and moments. A change in tyre resolution in simulations using FTire has negligible effects on simulation results, with only a change in processing time if the tyre resolution stays within the parameters set out by Cosin. The lateral and normal force results from the quarter car simulations were influenced the most by the change in road resolution. It is recommended that a 10x10mm resolution is used for quarter car simulations where the lateral and normal force is of high significance.

The full vehicle model shows very little changes in the reaction forces and moments when the resolution of the road is changed. It was found that the change in percentage error is negligibly small. And in the case of full vehicle simulations a 15x15mm road resolution is more than sufficient.

# Chapter 3: Micro texture

This section focuses on the tyre friction coefficient estimation based on the micro texture of the road. The first priority was to validate the estimation model on a flat road and then estimate the friction coefficient on the Belgian paving. Vertical displacement and speed were evaluated to determine what effects they would have on the friction coefficient results on the flat concrete and Belgian block. The Heinrich/Klüppel friction coefficient estimation model was used, with some of the Persson's model principles incorporated, such as the radially averaged PSD calculations. The viscoelasticity took into account the flash temperature by being dependent on the temperature and frequency shift. This temperature was measured using a FLIR Lepton camera. The estimations of friction coefficient are compared to experimental data and the road subsampled to determine the effects that a change in micro texture has on the results.

## 3.1 Experimental work

To validate that the friction estimation model is usable it has to be compared to experimental data. An experimental method based on Da, Vinci's friction model was used. The basic experimental setup can be seen in Figure 27, where the concrete block was mounted on top of a six component force table inside a CNC machine.

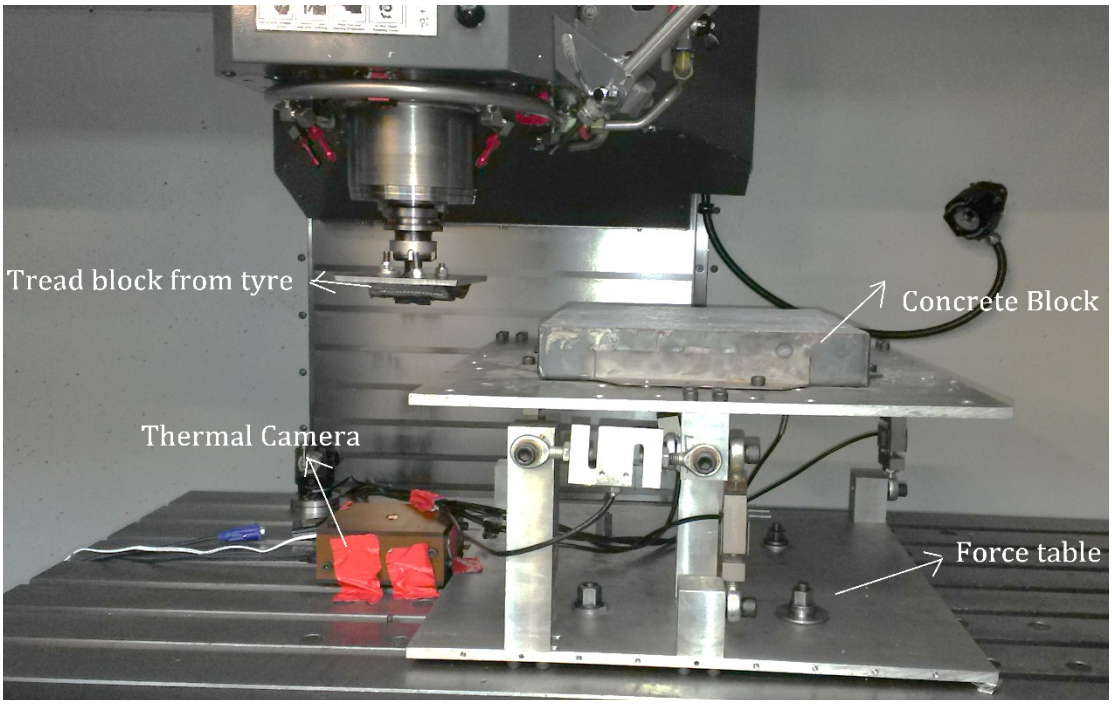


**Figure 27. Test setup to determine the friction coefficient**

The force table works in a similar manner as the WFT used in the previous section, just on a smaller scale. All the forces and moments are easily decoupled from each other since it is a non-rotating test setup. The force table consists of two parallel plates connected with the use of s-type load cells, placed in such a manner that the forces and moment in all three axis were measured. A schematic of how the load cells are positioned and can be seen in Figure 28.

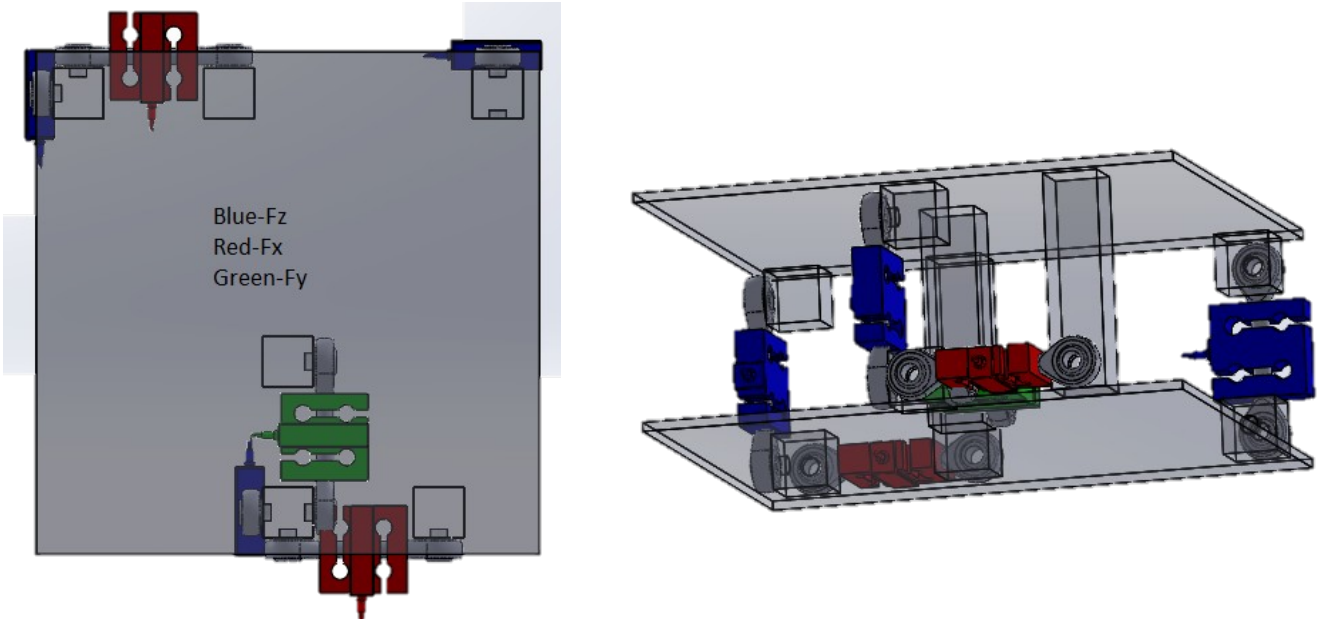


**Figure 28. Schematic of six component force table and which load cell measures which direction**

A thermal camera (Appendix A) was placed in a position where it would be able to take an image of the tread block as soon as it leaves the concrete block, to find an accurate temperature. The CNC machine was used as an actuator to control the tyre tread block to slide over the concrete block at specific speeds. A single tyre tread block was cut from the Michelin LTX/AT2 tyre. The tread block was completely isolated so that only this was in contact with the surface. The parameters that are significant to the study is the topography, the temperature of the tread block and the forces.

The experimental procedure starts off with the measurement of the temperature of the tread block, by taking a thermal image of it. The tread block is then pressed down unto either the flat concrete block or the Belgian paving. The block is pressed down to a pre-determined amount, before it is moved across the surface at various speeds, after which the CNC machine stops directly above the camera to take another thermal image. The tread block is then allowed to cool down before the next run.

### 3.1.1 PSD and topography

The micro texture is of small magnitude and is challenging to measure. Most road profile censoring capabilities stop at a macro scale, on the other hand, laser can measure at a micro scale and this is dependent on the size of the laser dot size. The smaller the measuring capability of a laser becomes, the higher the cost.

The profile of the concrete block was measured with the use of an Acuity AR700-8 laser (Appendix B) to enable the measurement of the micro texture topography. The laser was mounted inside the CNC spindle in such a manner that it could not rotate. The laser moves to the predetermined x- and y-coordinates in a grid pattern, at each of these positions the laser measures the height (z-coordinate) of the topography. Resulting in the micro texture of a surface measured at a 0.12x0.12mm resolution. The radially averaged PSD was found by using the calculations from the literature study, thus determining the top topography. The top topography was used throughout the rest of the calculations, since the friction coefficient is not effected by the bottom topography [ CITATION Kan17 \l 7177 ]. The new height of the topography can be seen in Figure 29. This height was now used to determine the correct PSD, known as the radially averaged top PSD determined from Equation 7 in section 1.1.2.

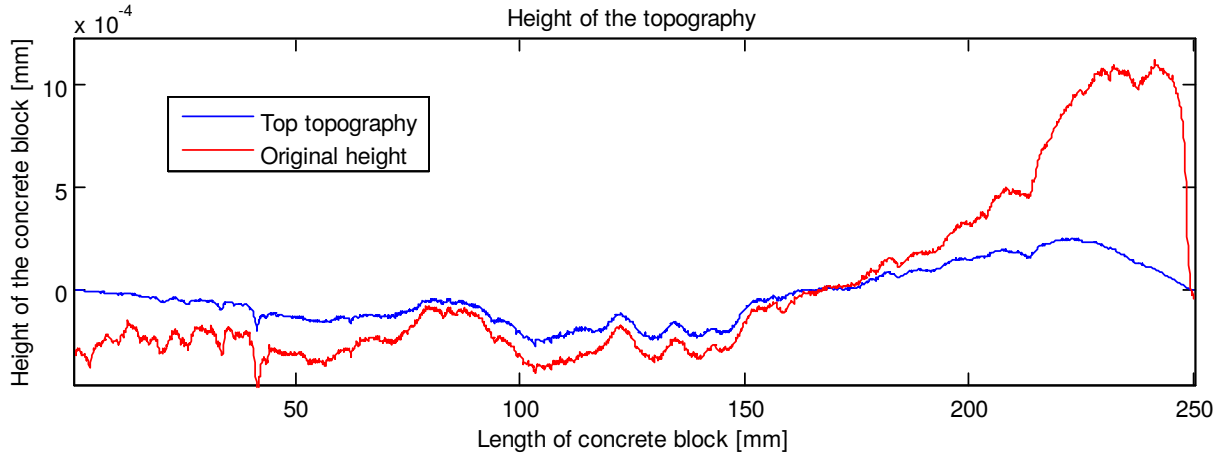


**Figure 29. Original and top topography**

## 3.1.2 Viscosity from the hysteretic loop

One of the important properties of the friction model, is the viscosity. The hysterectic loop was created to find the viscosity of the rubber tread block, since it was difficult to determine the properties for a composite rubber. To do this the tread block was attached to the CNC tool holder and pressed down vertically onto the concrete until it was compressed 2mm vertically. The tool holder was then oscillated in the x-axis between 3mm to -3mm. During these oscillations, the bottom part of the tread did not slide on the concrete and only the top part moved. From the forces in the x-axis a hysterectic loop was created, such as in Figure 30 for the full range of velocities (1-12 m/min).

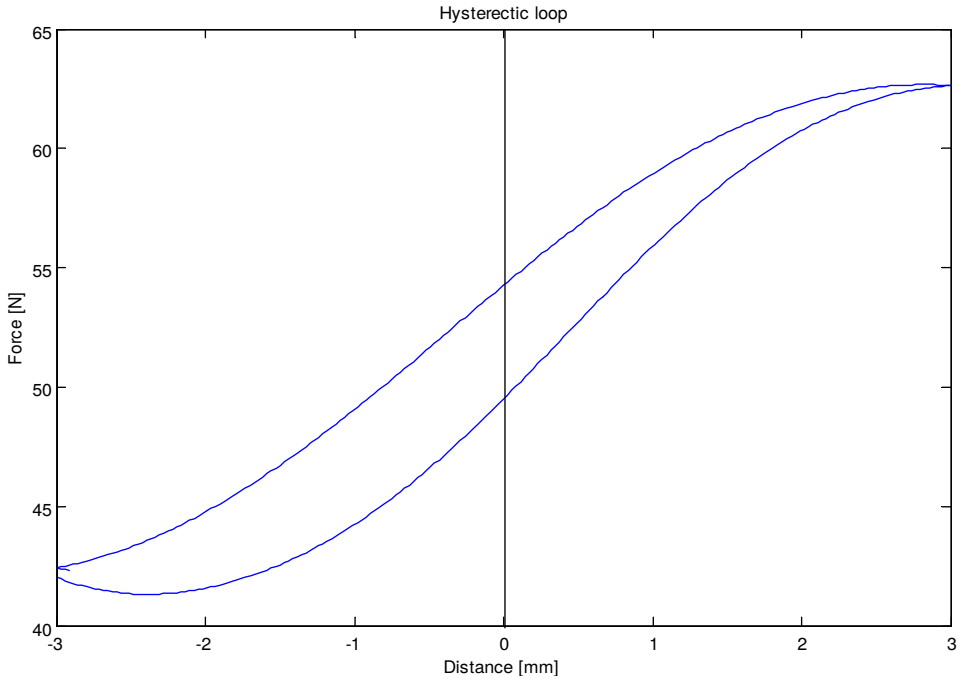


**Figure 30. Hysteretic loop for 1m/min**

The distance between the two lines in Figure 30 did not stay as constant as indicated in the literature study. This is why the $\Delta F$ was found where the x-axis was at zero. This force was multiplied with the velocity to find the damping coefficient. The damping coefficient was then plotted against the various velocities to create the damping coefficient as a function of velocity.

### 3.1.3 Contact area

The contact area would change with respect to the contact pressure. To determine what the contact area would be at a specific vertical displacement, the area of the tread block was painted and pressed down on to a piece of paper at a specific vertical displacement to create an imprint, as seen in Figure 31. The line above the imprint was used to determine a mm/pixel scale after the image was taken. The number of dark pixels were counted to determine the total area that the imprint created.

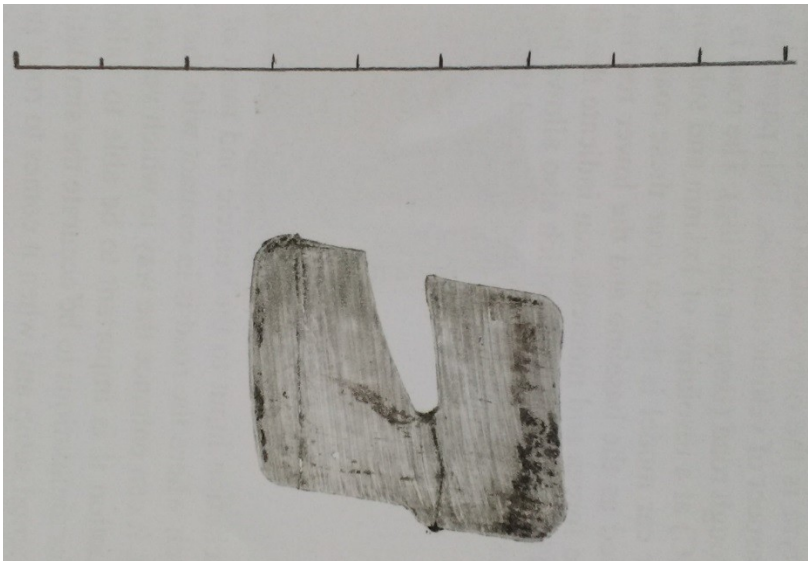

**Figure 31. Imprint of the tread block of 2mm displacement downwards**

### 3.1.4 Contact mechanics

The tyre penetration is dependent on the wavelength (λ) and this is used throughout the study. Based on findings from Persson's friction model [ CITATION BNJ06 \l 7177 ], the smallest wavelength are of the order 2pi/L, where L in this study is the lateral length of the tread block that was in contact with the road(32mm in this case). The largest wavelength is determined by 2pi/D, where D was the linear particle size of particles on the road surface. This wavelength in this study was limited by the measuring capability of the laser that was used to measure the surface. The laser dot is 120µm, thus limiting D to 120µm[ CITATION Acu15 \l 7177 ].

The integral for the friction estimation from equation 17 was over the laser dot size to the length of the tread block. This was done at 1mm increments to create a large number of friction coefficient estimations over the length of the surface. Thus every 1mm has a new friction estimation across the Belgian paving.

### 3.1.5 Flash Temperature

The aim of the thermal camera or in this case the FLIR Lepton camera (Appendix A) is to be able to detect the temperature of objects in a simplistic manner. The camera takes images and then creates a matrix using various values to represent the different temperatures for each pixel. To determine what temperature represents which pixel value, calibration was required. For this a glass was filled with hot water and as the water was left to cool down, images were taken every two minutes with the FLIR Lepton camera and also with a FLIR ThermaCam camera (Appendix A) to cover a full range of temperatures from a high temperature to room temperature. The ThermaCam alone was not used since it is large and an uncomfortable shape, where as the FLIR Lepton is small and easy to mount in various positions, it is also easier to use.

The ThermaCam adds temperature values directly to its pixels and this was then compared to the Lepton pixel values. There was a quadratic relationship between the temperature and the pixel values, as in

Figure 32. A quadratic function was fit to the data and is reflected on the figure. Multiple runs were completed to ensure that the quadratic fit was applicable in all cases. It was assumed that temperatures outside of the measured scope would follow the same trend.

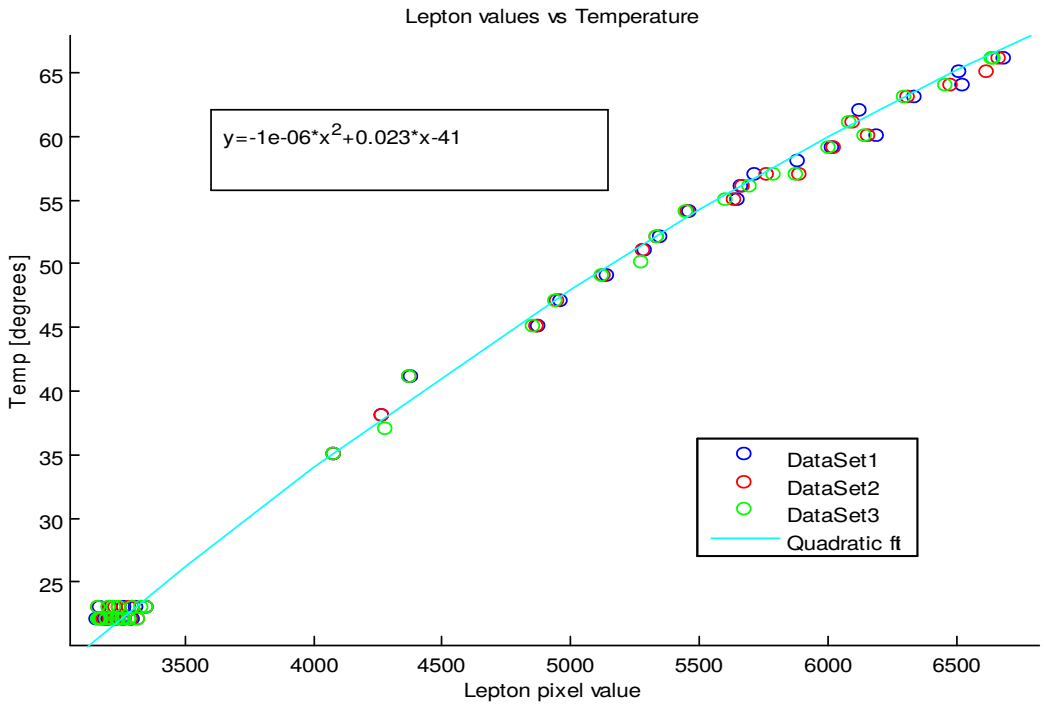


**Figure 32. Determining the function of temperature as a function of the pixel value**

A thermal image was taken of the tread block before and after each run as seen in Figure 33. The Images clearly show the tread block and how the temperature increased during the run. On the right image, it was clear that the one part of the tread block reached a higher temperature than the rest. The higher temperature section could be the section of the tread that overcame the static friction coefficient and dragged the rest of the block with it. Alternatively, the tread block was not completely flat and thus the one edge was pressed down more than the rest of the block.

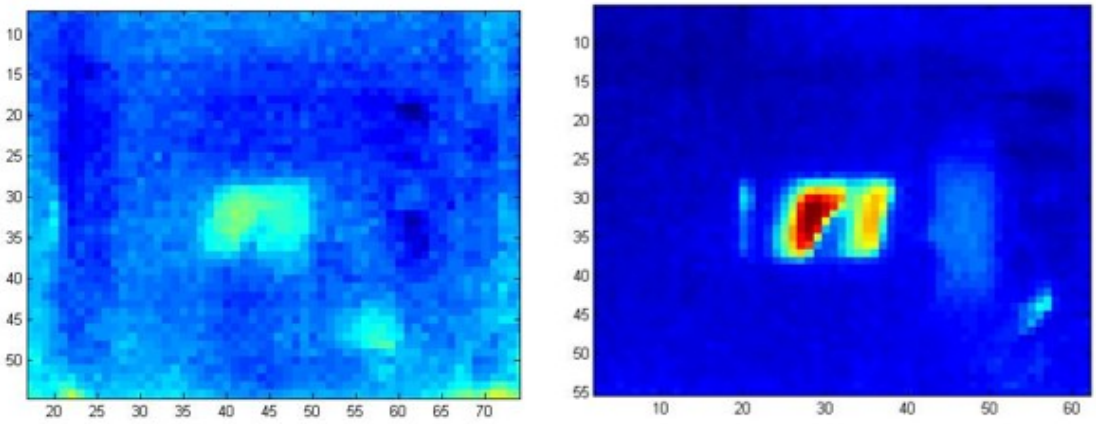

**Figure 33. Thermal images for before (left) and after (right) a 12m/min run**

The temperatures for the surface area was assumed to be more constant than indicated in Figure 33, since the FLIR Lepton camera scales the colour-map of the images according to the highest and lowest temperature. This was confirmed by a more detailed investigation of the pixel values, which showed a more even distribution of temperature over the tyre tread block. Based on the pixel values the

temperatures were averaged over the surface area to find the average viscoelasticity of the tread block. After every run, the tread block was given time to cool down back to its ambient temperature, to ensure that the previous run did not influence the temperature of the runs that followed. The initial measurement served as the ambient temperature and second measurement as the local surface temperature.

## *Flat concrete block*

The thermal images before and after each run were compared to each other. The change in temperature can be seen in Figure 34 for the various speeds and vertical displacement over the flat concrete block.

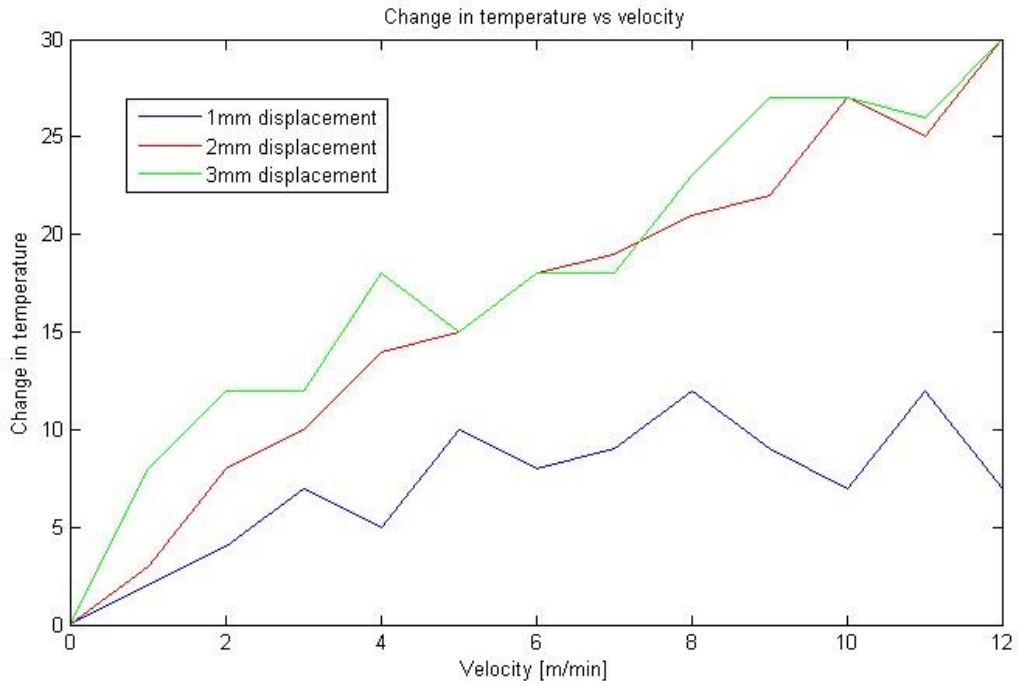


**Figure 34. Change in temperature for flat concrete block**

It was interesting to note that the change in temperature for 1mm vertical displacement fluctuates for the different speeds. This was caused by the noisy response measured in the friction coefficient as seen and discussed in section 3.2.1. The low displacement of rubber into the surface causes the rubber to not always be in contact with the surface and thus not always letting the temperature rise as expected. The average temperature change was low as expected, since the tyre was not in contact with all the asperities when vertically displaced with 1mm. The 2mm vertical displacement change in temperature reacted as anticipated, with a steady rise in temperature as the speed increased. Only the 10m/min was higher than the following speed. The average temperature was higher than that of the 1mm displacement. Once again the 3mm vertical displacement temperature results fluctuate slightly from 4m/min to 7m/min, however when the total temperature change was considered, the fluctuations were not significant. The average temperature was slightly higher that of the 2mm vertical displacement. The highest value of the two displacement were the same. It was interesting to note that the ambient temperature was higher than the glass transition temperature, indicating that this state was reached and thus the uncertain rubber to glass transition region was avoided.

## *Belgian Paving*

The test procedure for the Belgian paving is the same as for the flat concrete block, even though the tread block looses contact where one of the Belgian blocks stop and an another begins. The 1mm vertical

displacement had an extremely low change in temperature as seen in the summary in Figure 35, caused by the rubber barely touching any of the asperities on the surface of the Belgian paving. The change in temperature was also small when the vertical displacement was increased to 2mm and the temperature increased systematically up to 6˚C. The 3mm vertical displacement indicated that the temperature change was larger than that of 2mm vertical displacement. The temperature change increased consistently up to 12m/min and from 1mm to 3mm vertical displacement.

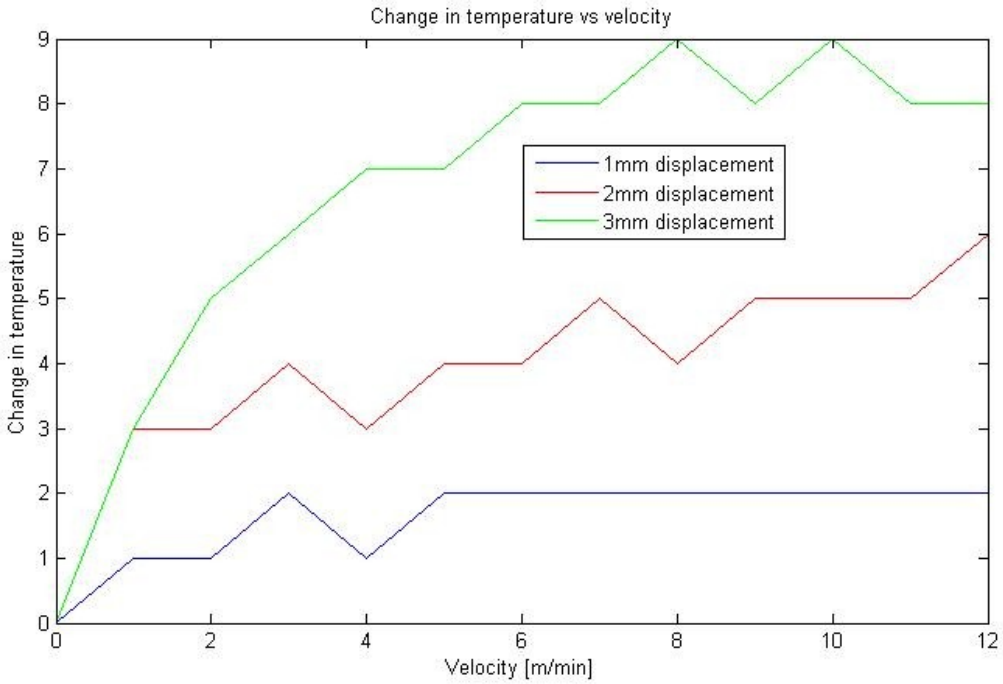


**Figure 35. Change in temperature for Belgian paving**

# 3.2 Validation of the friction model

The first block used was the flat concrete block and the second was the Belgian paving block. The tread block was placed on the blocks at a specific vertical displacement; the tyre tread was then moved at a known speed across the block. The forces were measured with the use of the load cells. To determine the experimental friction coefficient Equation 15.

## 3.2.1 Estimation and experimental data discussion

Since the forces already included the various velocities (1m/min to 12m/min), the friction coefficient ($\mu_k$) was found by dividing the lateral force ($F_x$) by the vertical force ($F_N$) as in Equation 24 resulting in Figure 36 for the 1mm vertical displacement.

$$\mu_k = \frac{F_x}{F_N} \qquad 24$$

As expected, initially the friction coefficient was close to zero; it then climbed steeply due to static friction and levelled out at one as the static friction was overcome. The trend line in each figure indicates the average of the experimental data. The friction coefficient data jumped to large magnitudes; this was caused by the 1mm vertical displacement being a small amount. The rubber was not slipping over the surface at a constant rate, in turn causing a high frequency, which causes the large magnitudes.

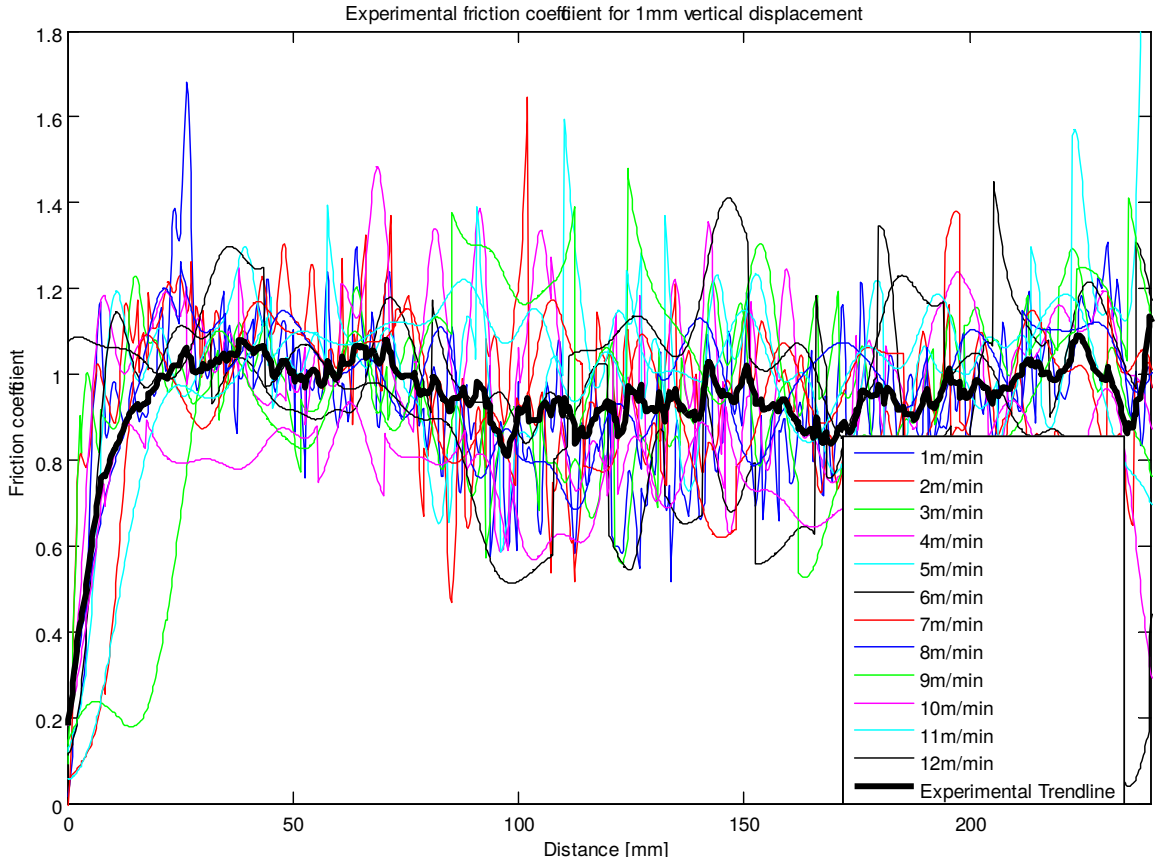


**Figure 36. Experimental friction coefficient for 1mm vertical displacement**

The mathematical estimation results can be seen in Error: Reference source not found determined from Equation 15. The general trend of the results seems to often deviate with large numbers. The trend line was determined by taking the average of all the different speeds combined. The average of the data reflected the opposite, with the coefficient of friction value of one, as in the experimental data in Figure 36. This was also indicated when comparing the experimental trend line to the estimation of the friction coefficient. The estimation also showed the same frequency caused by the rubber not slipping at a constant rate. The topography is also shown in Figure 37 to show how it correlates to the friction coefficient values. This showed that even though the height of certain parts of the topography changed, the friction coefficient was not dependent on this.

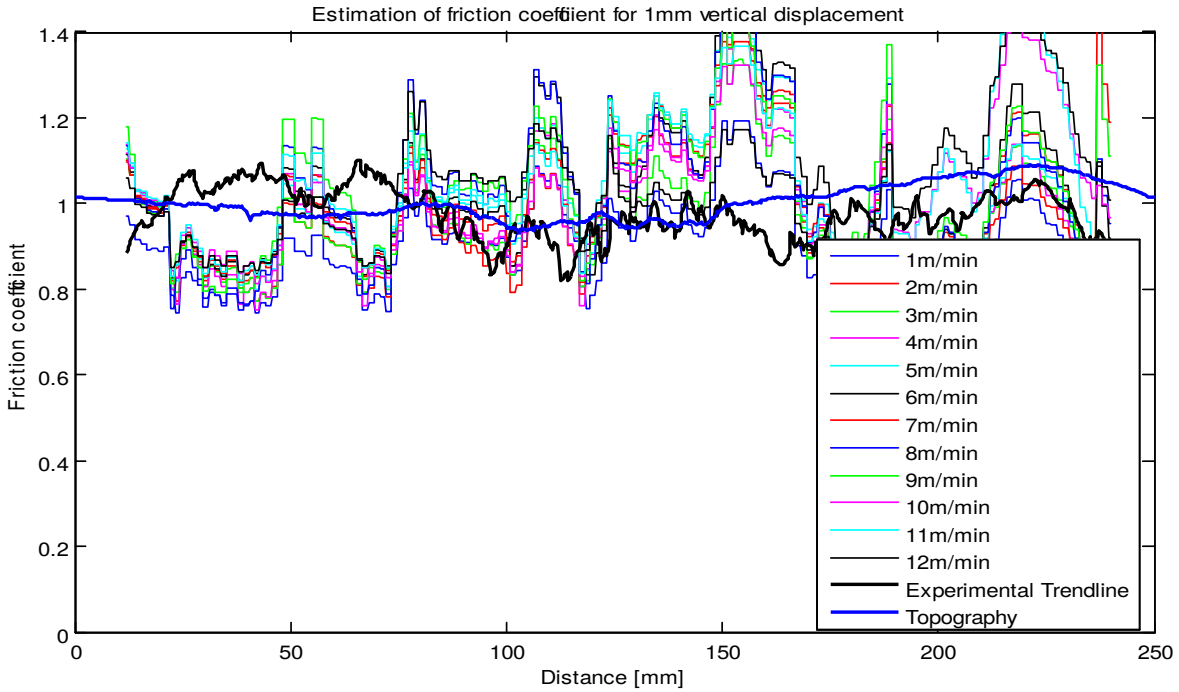


**Figure 37. Estimation of friction coefficient of 1mm vertical displacement**

When the tread block was vertically displaced by 2mm, the friction coefficient found experimentally had a lower magnitude when compared to the 1mm vertical displacement. The same trend as for the 1mm vertical displacement was seen in Figure 38, where the static friction was overcome and it leveled out at one. The friction coefficient estimation (Figure 39) for 2mm vertical displacement reflected the experimental data significantly better than for the 1mm vertical displacement results. This was seen from how closely the estimation followed the experimental trend line.

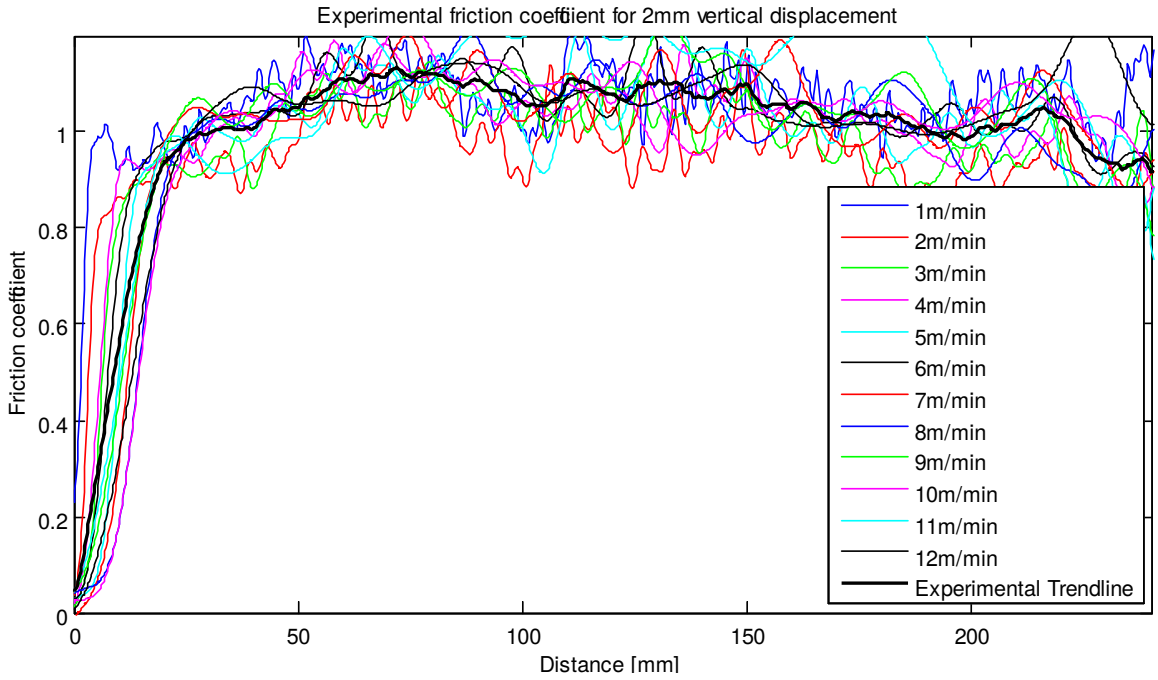


**Figure 38. Experimental friction coefficient for 2mm vertical displacement**

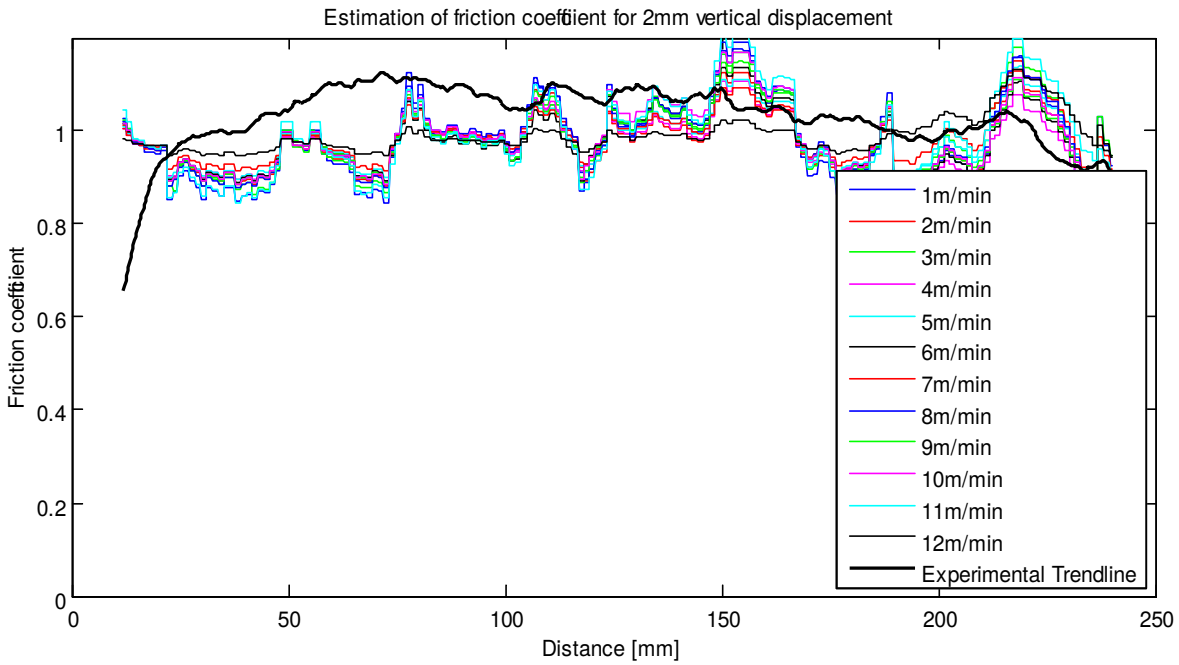


**Figure 39. Estimation of friction coefficient for 2mm vertical displacement**

Experimental data was used to calculate the friction coefficient for 3mm vertical displacement as seen in Figure 40. The friction coefficient oscillated much less compared to the previous two results. The same was seen in Figure 41 for the friction coefficient estimation. The various speed results were also closer to each other, with a better average.

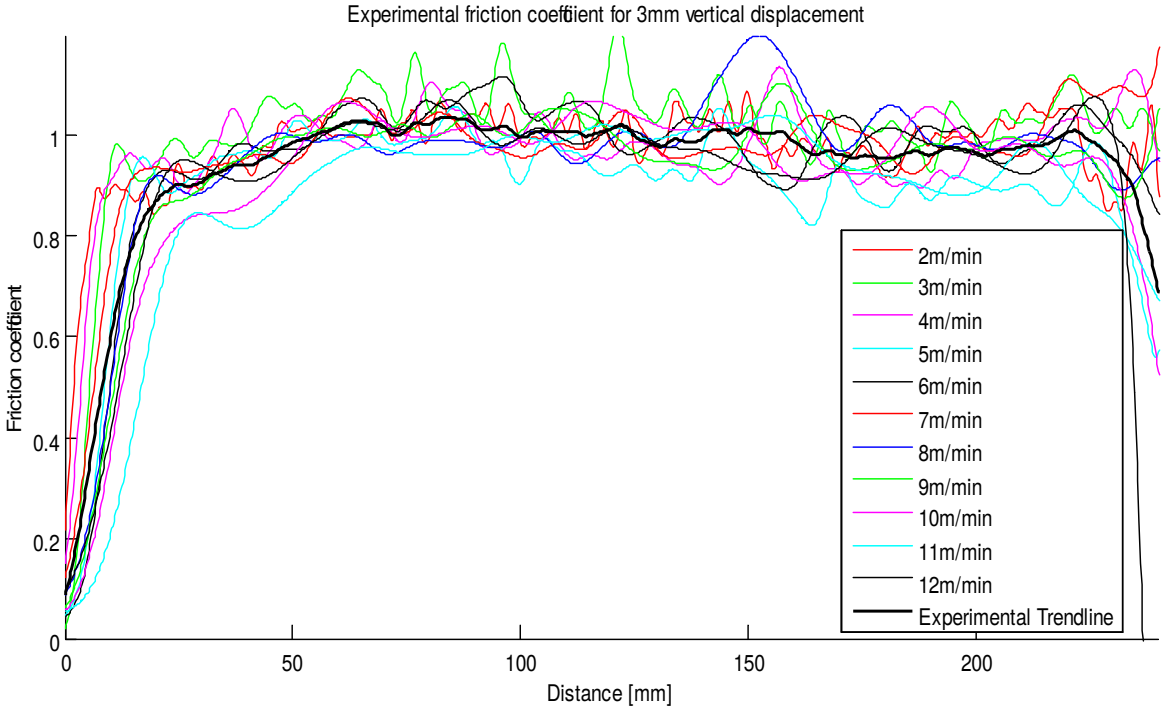


**Figure 40. Experimental friction coefficient for 3mm vertical displacement**

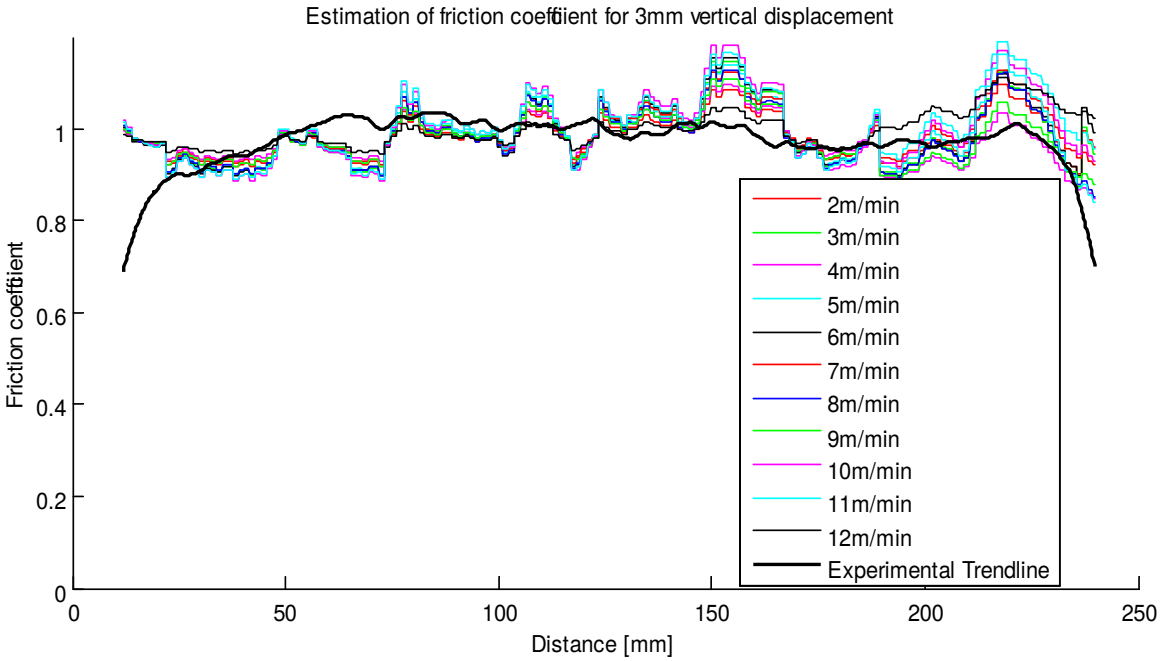


**Figure 41. Estimation of friction coefficient for 3mm vertical displacement**

## 4.2.2 Trend lines

The experimental trend line is the average of the various speeds of the various velocities approximated for each different vertical displacement. The trend lines as seen in figure, all start as approximately zero and followed the same general trend. This indicates consistency throughout the tests. The topography was scaled and plotted in Figure 42. This was done to investigate how the friction coefficient related to the shape of the concrete block. The topography indicated that the friction coefficient correlated to it and followed a constant value. The 1mm vertical displacement trend line peaked at one and then dropped down slightly, while the 2mm vertical displacement peaked to above one. The 3mm vertical displacement stayed more constant over the surface length when compared to the others.

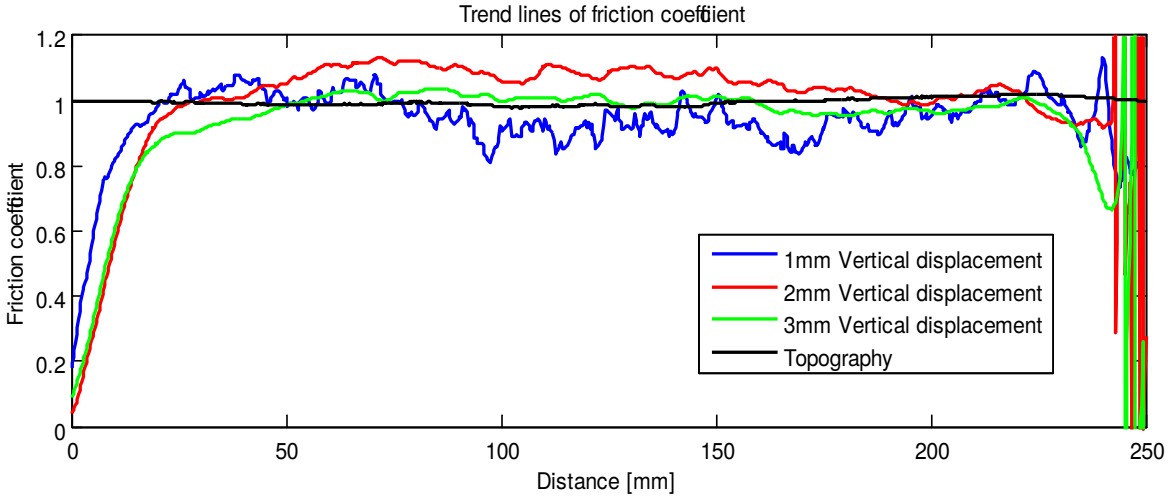


**Figure 42. Trend lines of vertical displacements for friction coefficient over concrete block**

### 3.2.3 Effects of vertical displacement

In Figure 43 the various vertical displacements were investigated at a speed of 1m/min. The 1mm vertical displacement showed a high frequency and high magnitude, this decreased as the vertical displacement increased. This was influenced mainly by the surface area, since this affects how deep the rubber penetrated in to the surface texture, which in turn reduced the frequency of the rubber as it slipped. The same trends were followed for the higher velocities.

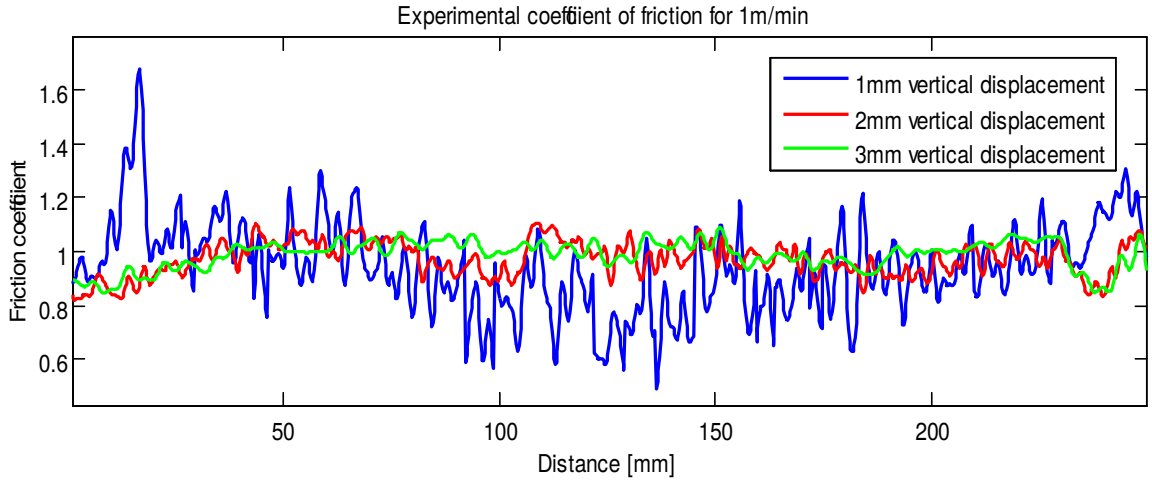


**Figure 43. Effect of vertical displacement on the friction coefficient on the concrete block**

### 3.2.4 Effects of velocity

As the velocity of the tread block over the concrete increased, the frequency of oscillation decreased (Figure 44) over the length. Figure 44 showed a decrease in amplitude caused by the increase in velocity. This can also be seen as the tread block not 'seeing' all the details of the block since it was moving too fast across the surface. This was expected to influence the percentage error in section 2.2.5.

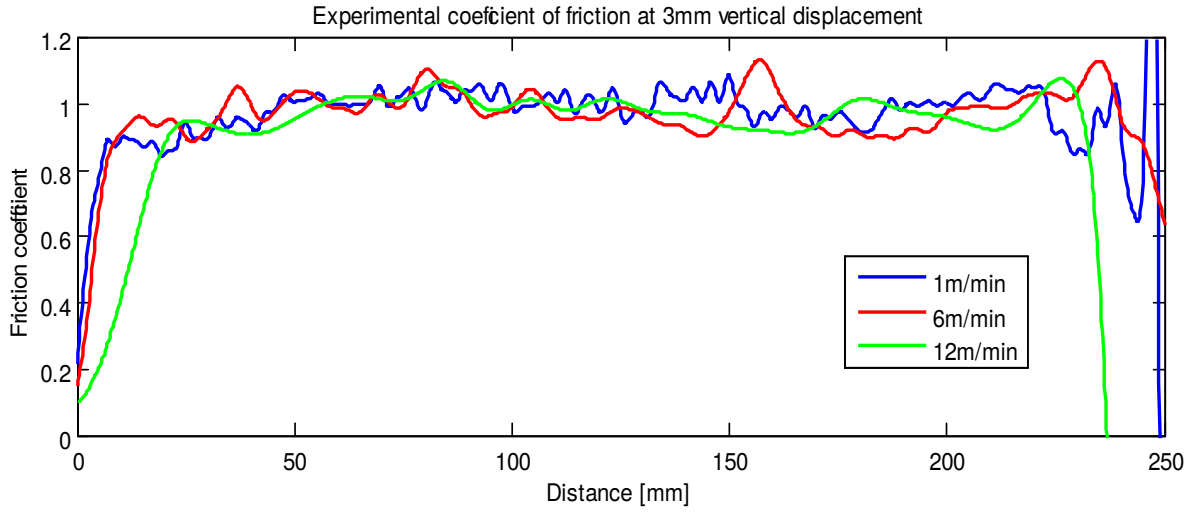


**Figure 44. Effects of velocity on the friction coefficient on the concrete block**

## 4.2.5 Percentage error

The percentage error, from equation 22 of the estimation and experimental data compared to the experimental trend lines of each vertical displacement was used to indicate how accurate the Heinrich/Klüppel model was, as seen in summary in Table 6.

**Table 6. Percentage error of estimation and experimental friction coefficient compared to a coefficient of one**

| Velocity (m/min) | 1mm displacement | | 2mm displacement | | 3mm displacement | |
|---|---|---|---|---|---|---|
| | Estimation | Experimental | Estimation | Experimental | Estimation | Experimental |
| **1** | 16 | 15 | 11 | 8 | 7 | 5 |
| **2** | 18 | 15 | 10 | 9 | 6 | 5 |
| **3** | 16 | 13 | 10 | 7 | 7 | 8 |
| **4** | 18 | 16 | 10 | 5 | 6 | 8 |
| **5** | 19 | 19 | 9 | 6 | 8 | 7 |
| **6** | 20 | 18 | 10 | 5 | 8 | 5 |
| **7** | 18 | 14 | 9 | 5 | 7 | 7 |
| **8** | 21 | 21 | 10 | 6 | 7 | 7 |
| **9** | 19 | 26 | 10 | 5 | 6 | 5 |
| **10** | 18 | 9 | 9 | 7 | 9 | 6 |
| **11** | 20 | 13 | 11 | 11 | 8 | 9 |
| **12** | 18 | 27 | 9 | 8 | 7 | 5 |

For the 1mm vertical displacement, the percentage errors were below 30% for both the experimental and estimation data. The experimental percentage error was lower than that of the estimation; however, it only varied with ±10%. It varied for the numerous speeds at random; this again was caused by the large frequency and magnitude of the data at 1mm vertical displacement. The 2mm vertical displacement showed similar results, with the percentage error being larger for the estimation that for the experimental data varying with <10%. The results were much more consistent with smaller variations than the 1mm vertical displacement. The 3mm vertical displacement percentage error was close to the values of the 2mm vertical displacement for the experimental data. The experimental and estimation percentage error were much closer to each other and only vary with <5% for the 3mm vertical displacement. Showing once again that the as the vertical displacement increased, so does the accuracy of both the experimental and estimation data.

## 3.2.6 Effects of road resolution

Since the 3mm vertical deflection is the most accurate, only these results were used to evaluate the effects of the road resolution. The road was measured at a 0.12x0.12mm resolution and subsampled, through a basic interpolation, to resolutions of 0.144, 0.168, 0.192, 0.216 and 0.240mm. To ensure that the subsampling was done correctly, Figure 45 was created. Since the road could not be sampled smaller than this, no conclusion could be made for anything smaller than 0.12mm. This plotted the subsampled data and the original resolution to be compared to one another. Figure 45 represents a zoomed section of a specific section of the topography to indicate that when the road resolution was increased, the less micro texture was seen in the form of asperities. It is clear that the black line looses texture details up to a point where it is smooth and this was selected as the largest resolution evaluated. The range of micro texture resolution evaluated falls within the micro texture scale of smaller than 0.5mm. From the figure it is seen that for the flat concrete block the 0.240mm is more than sufficient enough and that the scale from 0.240mm to 0.5mm would have little effect on the results.

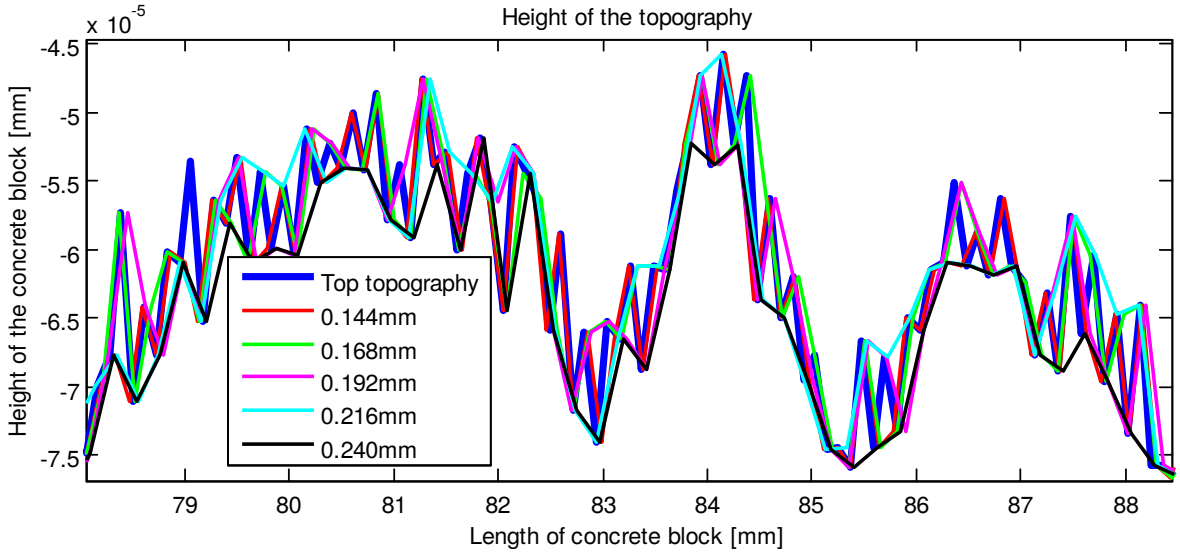


**Figure 45. Topography of the flat concrete and it's subsampled data**

Table 7 represents the percentage error of the friction estimation for the various road resolutions compared to the experimental friction coefficient trend line. The 0.144 showed an increase in percentage error, so did all the larger resolutions. The error fluctuates between the speeds, however stays within 5% error for each change in road resolution. The largest resolution inspected had the largest percentage error of close to 20%. Thus the 0.216 resolution is considered to be the limit of the micro texture on a flat road.

**Table 7. The effect of the road resolution on friction coefficient estimation error on the flat concrete block**

| Velocity (m/min) | Road resolution (mm) | | | | | |
|---|---|---|---|---|---|---|
| | 0.120 | 0.144 | 0.168 | 0.192 | 0.216 | 0.240 |
| **2** | 6 | 10 | 12 | 9 | 9 | 13 |
| **3** | 7 | 12 | 14 | 14 | 12 | 20 |
| **4** | 6 | 11 | 15 | 9 | 8 | 12 |
| **5** | 8 | 12 | 16 | 14 | 11 | 18 |
| **6** | 8 | 11 | 14 | 12 | 12 | 18 |
| **7** | 7 | 10 | 13 | 8 | 10 | 15 |
| **8** | 7 | 12 | 14 | 13 | 11 | 18 |
| **9** | 6 | 11 | 14 | 9 | 9 | 13 |
| **10** | 9 | 12 | 16 | 15 | 12 | 21 |
| **11** | 8 | 13 | 15 | 14 | 12 | 21 |
| **12** | 7 | 12 | 15 | 10 | 8 | 10 |

Figure 46 is a graphical representation of the effect that the road resolution has on the friction coefficient. From this it was also clear that the resolution smaller than 0.240mm, follower the same trend as that for the original resolution, and the 0.240mm reaches peaks of 1.2, which has large effects on the vehicle dynamics. Confirming that for a flat road the 0.216mm is the limiting micro texture resolution.

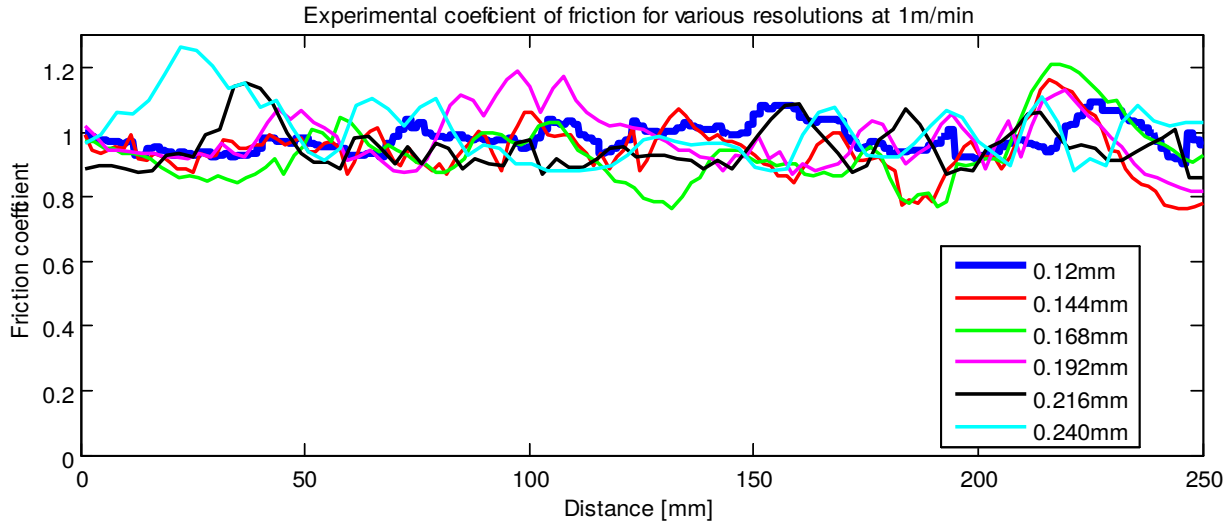


**Figure 46. Friction coefficient estimation for various road resolutions at vertical deflection of 3mm and at 1m/min over a flat concrete block**

# 3.3 Belgian Paving

The Heinrich/ Klüppel friction coefficient estimation was validated in section 3.2 on the flat concrete block. Even though both Person's and the Heinrich/ Klüppel model states that their models should be valid over a wide range of road roughness's, it has not been tested on a road as rough as the Belgian paving. This section is aimed at repeating the tests in section 2.2 on a segment of the Belgian paving, to determine if the estimation would work and also what effect the micro texture resolution would have on these estimations.

## 3.3.1 Topography

Once again, only the top topography was considered, excluding the irrelevant rise and fall of the pavement topography that do not contribute to the road friction [ CITATION Kan17 \l 7177 ]. Figure 47 indicates the influence that the radially averaged topography has on the Belgian paving profile. It is interesting to note that the top topography decreases the large asperities in the form of height and valleys. It was necessary to compensate for the large difference in height of the topography with the vertical displacement that the tyre tread block followed. The vertical displacement was adjusted to ensure that the displacement was consistent over the length of the topography.

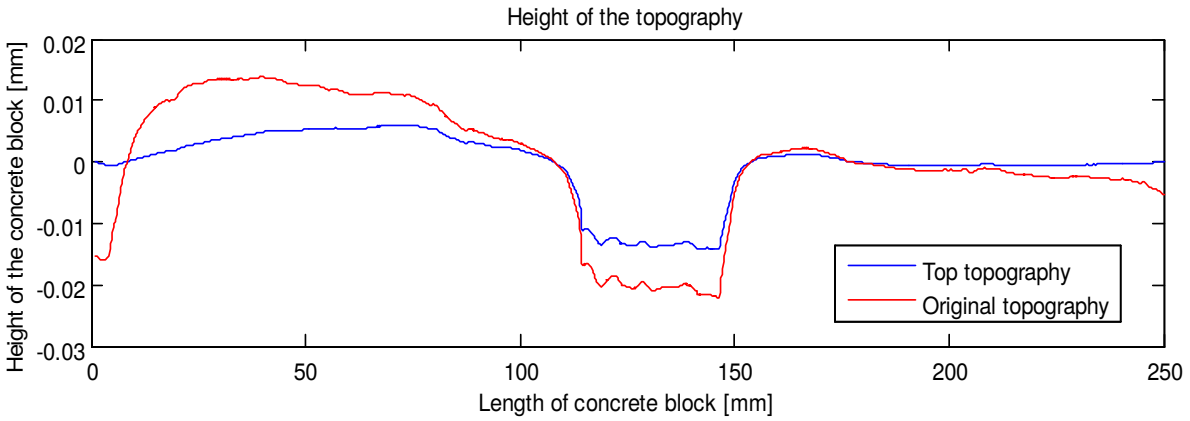


**Figure 47. Original and top topography (bottom) and the actual two blocks that the simulations are run across (top)**

## 3.3.2 Estimation and experimental data discussion

The 1mm vertical displacement was not considered. This is mainly due to the tyre tread barely touching the paving in some places, which resulted in poor results with no significant patterns of form and it could not contribute to the study. This was confirmed by the small increase in temperature seen from the flash temperature.

The 2mm vertical displacement experimental results can be seen in Figure 48, where a clear pattern is seen. The friction coefficient starts at zero and climbs steeply as static friction is overcome, as expected. The first block has a friction coefficient of ±1.3 and the second block with ±1.5, with an obvious valley in-between where the coefficient dips to zero as the tread block leaves the surface. When the friction coefficient is compared to the trend line, there are large peaks in the data.

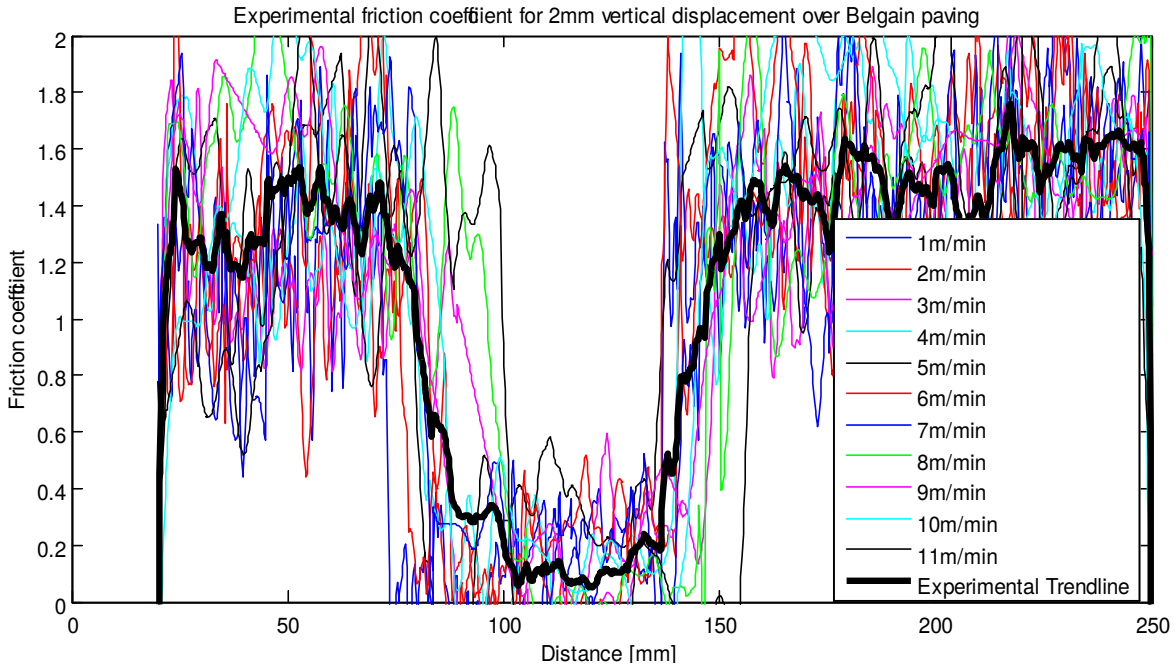


**Figure 48. Experimental friction coefficient for 2mm vertical displacement over Belgian paving**

Figure 49 shows the estimation of the friction coefficient based on the Heinrich/Klüppel model. The topography was scaled to fit on the same curve as the estimation data to indicate how it compared to the friction coefficient curve. The experimental trend line started at roughly 20mm on x-axis while the topography starts at zero. This is done to start the tread block on top of the surface to indicate how the static friction was overcome. The same rough pattern was seen for the estimation when compared to the experimental results, with some large magnitudes (Figure 49). The first blocks estimation shows a poor correlation of 1.2, with a deep valley and a better estimation of the second block's 1.5 friction coefficient. The estimation of the valley however is shaped too narrowly compared to the trend line and the topography. This can be explained by the way in which the tyre tread block was modeled. The model was perceived to deflect the same amount over the entire area of the tread block, even if only the edge of the tread was in contact with the surface. When the trend line was compared to the topography, it was seen that for the first block even the experimental data calculated the valley too large. This could be caused by the tread block having poor contact with the surface because of the large asperities on the surface.

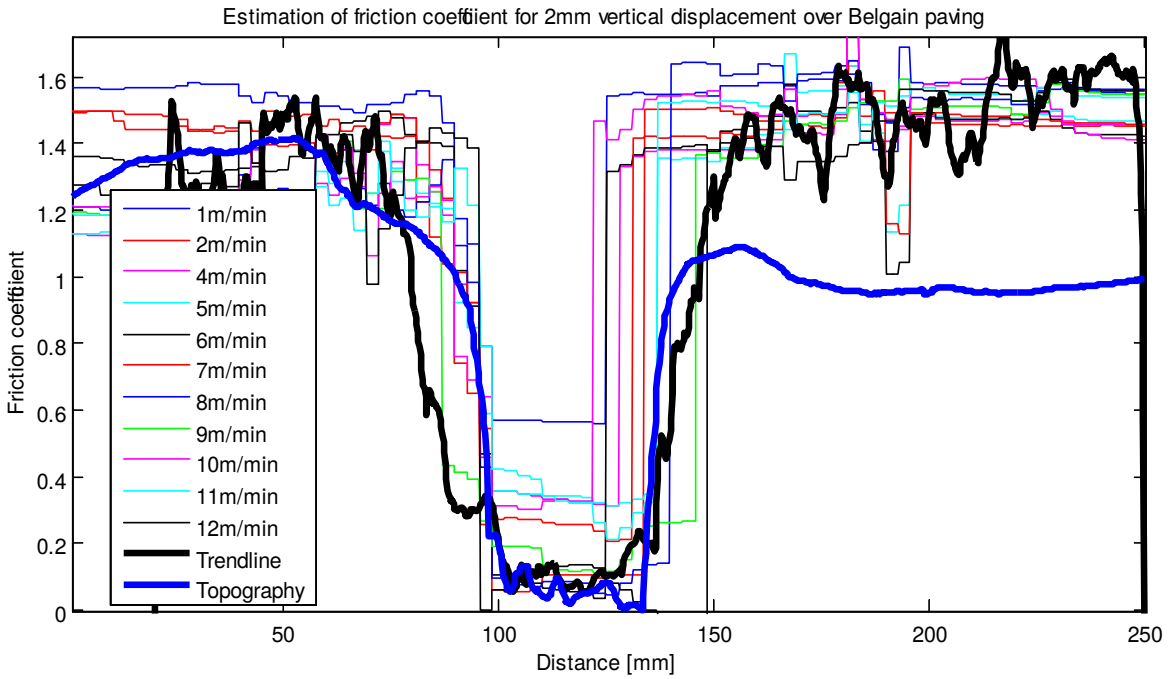


**Figure 49. Friction coefficient estimation for 2mm vertical displacement over Belgian paving**

The tread block was subsequently displaced with the 3mm and the friction coefficient determined experimentally, with the results seen in Figure 50. The same pattern is seen as for the 2mm vertical displacement, with slightly lower noise frequencies and magnitude. The first block again indicates a 1.2 friction coefficient and the second block a 1.5, however it rises to almost two at the end of the second block.

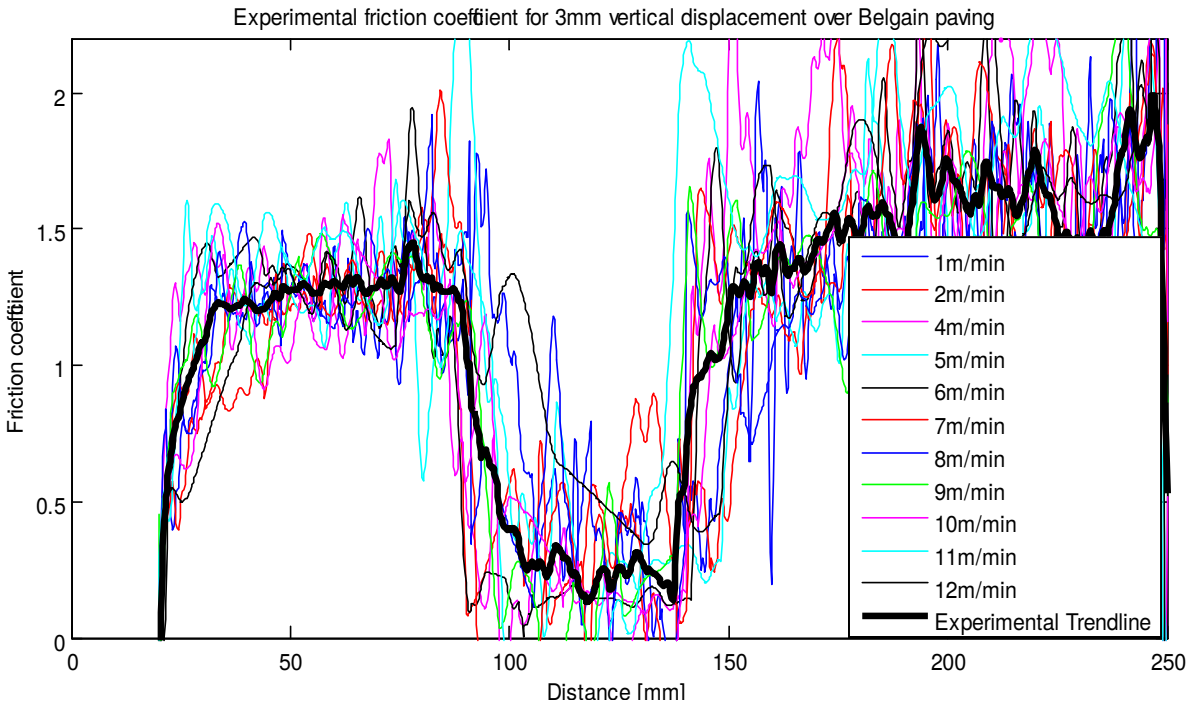


**Figure 50. Experimental friction coefficient for 3mm vertical displacement over Belgian paving**

The estimation of 3mm vertical displacement is shown in Figure 51. The estimation follows the experimental data closely with low magnitudes. The estimation of the friction coefficient again estimated the valley too narrowly, due to how the tyre tread was modeled. The valley followed a closer pattern to the experimental trend line. The last 50mm where there were high peaks on the trend line. In this case, the trend line followed the topography better than for the2mm vertical displacement, due to the narrow valley.

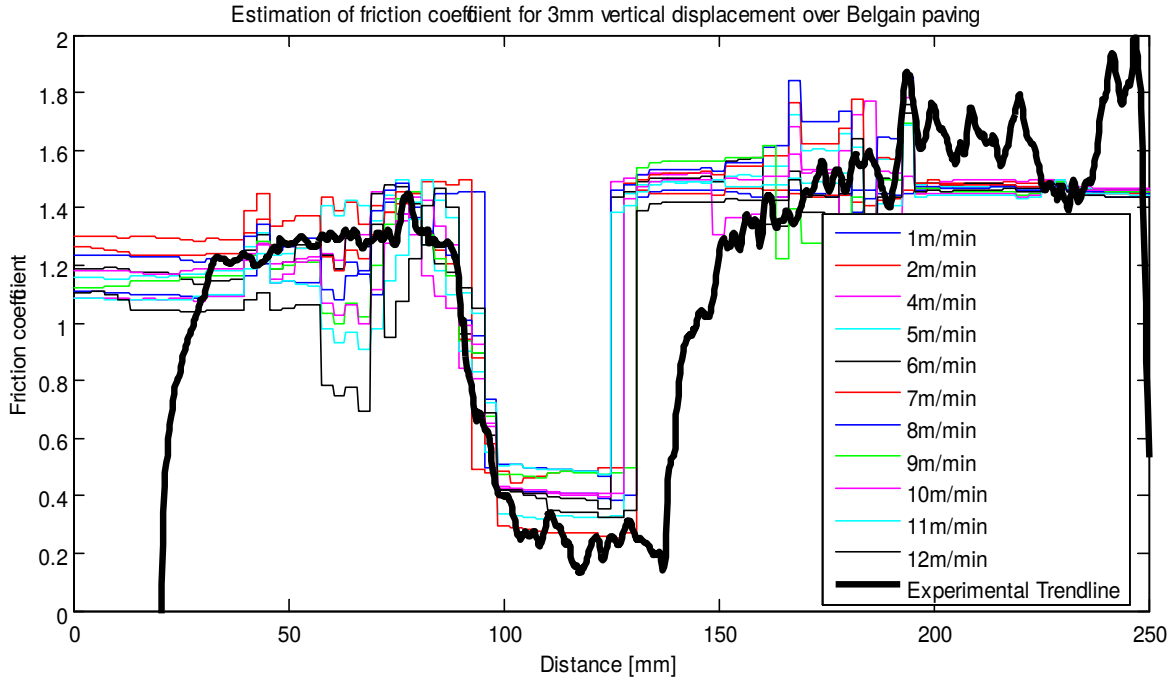


**Figure 51. Estimation of friction coefficient for 3mm vertical displacement over Belgian paving**

## 3.3.3 Trend lines

The experimental trend lines for the 2mm and 3mm vertical displacements are depicted in Figure 52. The 2mm vertical displacement shows high magnitudes on the first block, a valley that occurs to early and lower peaks on the second block. The trend line for the 3mm vertical displacement shows better results for the first block with a valley in the correct place, but higher amplitudes on the second block. This could be caused by the tyre tread detecting more details of the paving when it penetrates deeper into the asperities. When the results are compared to the topography line, the 3mm trend line followed a better description of the surface topography.

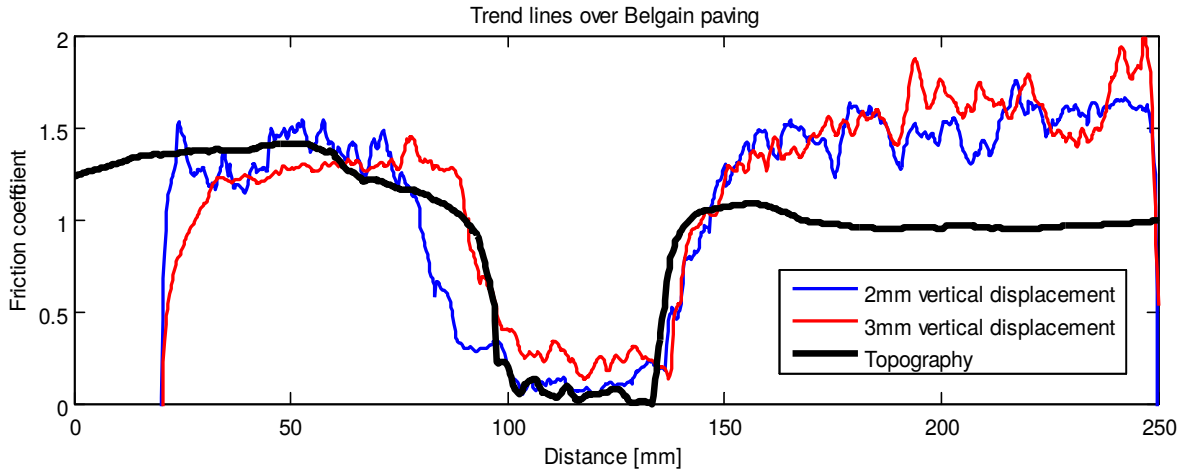


**Figure 52. Experimental trend lines of vertical displacements for friction coefficient over Belgian paving**

## 3.3.4 Effects of vertical displacement

The effects that the vertical displacement has on the results can be seen in Figure 53. The 2mm vertical displacement shows a high amplitude on the first block and dips into the valley too early as also seen in the trend line. The 3mm vertical displacement has smaller amplitudes on the first block and a better average on the second block, still with large magnitudes. The vertical displacement did not have as large of an effect on the Belgian paving as it did on the flat concrete block. This is because of the size of asperities on the surface.

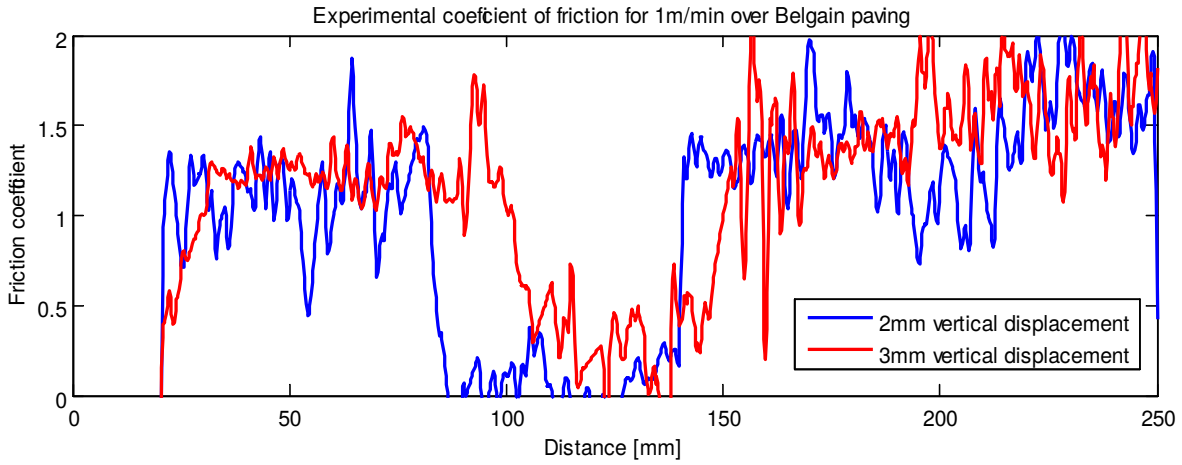


**Figure 53. Effect of vertical displacement on the friction coefficient on the Belgian paving**

## 3.3.5 Effects of velocity

The frequency of the 'noise' decreases, as the velocity increases, as seen in Figure 54. Both the 1m/min and 6m/min have large magnitudes while the 12m/min has smaller and smoother results. The general trend is kept throughout the different velocities. The velocity did not have as large of an effect on the Belgian paving as it did on the flat concrete. However, the highest velocity also reflects a lower frequency and magnitude, confirming that as the velocity increases, less detail of the surface is detected by the tyre tread.

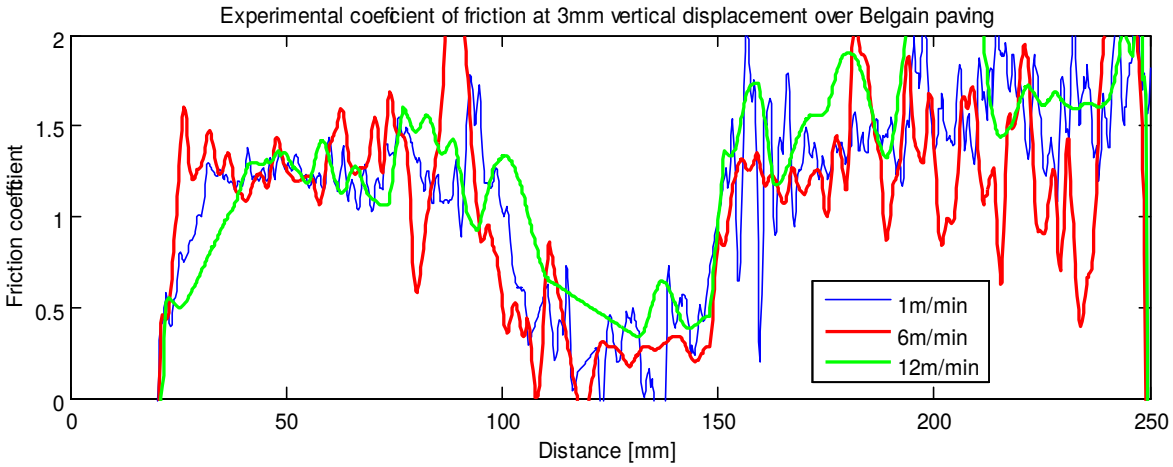


**Figure 54. Effects of velocity on the friction coefficient on the Belgian paving**

## 3.3.6 Percentage error

This data is analysed in more detail in Table 8, where the percentage error, from equation 22 was calculated between the experimental trend line and the estimation data. Since the friction coefficient changed over the paving blocks, the data is compared to the experimental trend lines.

**Table 8. Percentage error of estimation and experimental friction coefficient compared to the average friction coefficient**

| Velocity (m/min) | 2mm displacement | | 3mm displacement | |
|---|---|---|---|---|
| | Estimation | Experimental | Estimation | Experimental |
| **1** | 47 | 30 | 27 | 23 |
| **2** | 41 | 24 | 27 | 22 |
| **3** | 40 | 25 | 27 | 24 |
| **4** | 41 | 27 | 26 | 27 |
| **5** | 43 | 29 | 23 | 31 |
| **6** | 44 | 31 | 26 | 20 |
| **7** | 44 | 26 | 23 | 26 |
| **8** | 43 | 33 | 28 | 24 |
| **9** | 37 | 21 | 25 | 20 |
| **10** | 41 | 30 | 26 | 18 |
| **11** | 52 | 46 | 29 | 35 |
| **12** | 44 | 30 | 26 | 29 |

The 2mm vertical displacement shows poor results for the experimental and estimation data, with a difference between them of ± 20%. The high values of the percentage error for the estimation and experimental data is caused by the high frequency of the Belgian paving. The percentage error of the 3mm vertical displacement is lower than that of the 2mm results with roughly 10%. The difference between the experimental and estimation percentage error is less than 10%. Some of the estimation data is determined to have a smaller percentage error than the experimental data.

## 3.3.7 Effect of road resolution

The Belgian paving was also subsampled at the same resolutions as the flat road and the percentage error investigated with the results seen in Table 9. The road resolution effected the percentage error in an unexpected manner indicating that the 0.144mm resolution is the same as that for the 0.120mm resolution. The 0.168mm and 0.192mm resolution shows an increase in percentage error and it decreases again at the 0.216mm resolution. The smallest road resolution was once again limited by the size of the laser dot, which is 0.120mm.

**Table 9. The effect that road resolution has on the percentage error between the friction coefficient estimation data of the Belgian paving block**

| Velocity (m/min) | Road resolution (mm) | | | | | |
|---|---|---|---|---|---|---|
| | 0.120 | 0.144 | 0.168 | 0.192 | 0.216 | 0.240 |
| 1 | 27 | 26 | 30 | 32 | 30 | 29 |
| 2 | 27 | 26 | 33 | 36 | 30 | 33 |
| 4 | 26 | 26 | 35 | 35 | 31 | 35 |
| 5 | 23 | 25 | 37 | 32 | 26 | 29 |
| 6 | 26 | 26 | 40 | 31 | 29 | 34 |
| 7 | 23 | 27 | 34 | 39 | 29 | 35 |
| 8 | 28 | 26 | 36 | 38 | 29 | 31 |
| 9 | 25 | 25 | 33 | 35 | 29 | 36 |
| 10 | 26 | 27 | 34 | 32 | 23 | 28 |
| 11 | 29 | 28 | 31 | 33 | 32 | 29 |
| 12 | 27 | 27 | 34 | 39 | 27 | 29 |

The estimations of the friction coefficient for the various road resolutions can be seen in Figure 55. It is significant that the estimation for the second block is very reliable. On the other hand, the estimation for the first block is very poor. Half of the estimation was accurate and the other half was not, this could explain the fluctuations in the percentage error results between the various resolutions. This could be caused by the rubber being cold and taking the first paving block to 'warm up' and thus having more accurate results for the second block of paving once it is 'warmer' and thus more consistent.

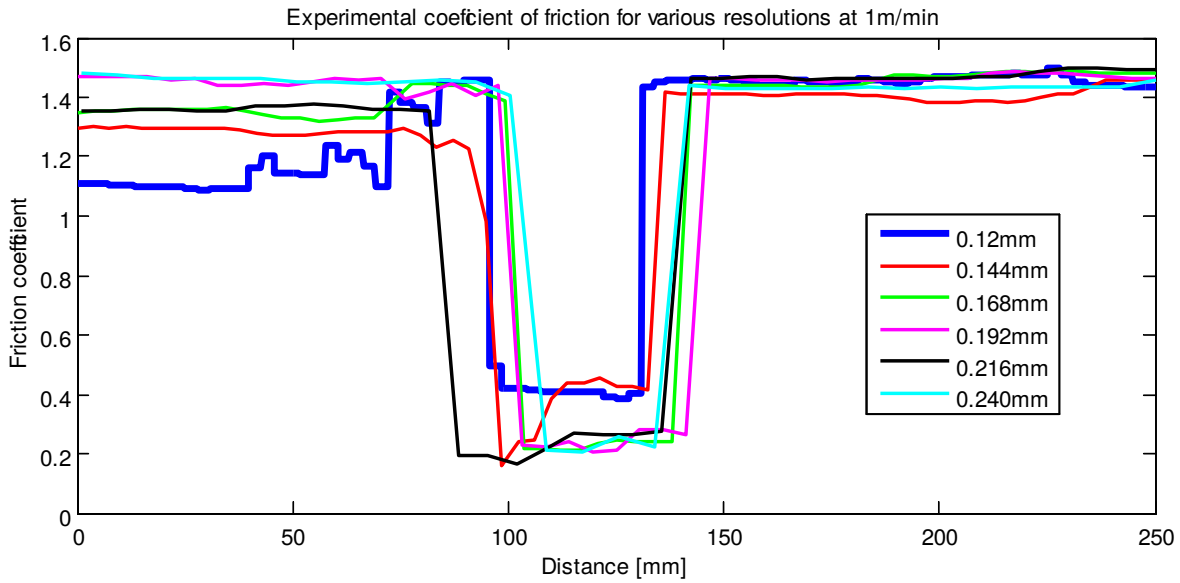


**Figure 55. Friction coefficient estimation for various road resolutions at vertical deflection of 3mm and at 1m/min over Belgian paving block**

## 3.4 Comparison to a full tyre model

Since only a small portion of an actual tyre is investigated in this study, the question arises of how implementable this would be on a tyre. A previous evaluation done with the use of the Heinrich/Klüppel model, with the results shown in Figure 56, attempted to predict the friction number on a flat road

[ CITATION LiL16 \l 7177 ]. The measured data is compared to the predicted friction number. The friction number directly correlates to the friction coefficient and was used in this study instead of the friction coefficient. The relationship between the measured and predicted FN's, the linear regression is used. Findings indicate a good correlation between measured and predictions with $R^2 = 0.79$ [ CITATION LiL16 \l 7177 ]. This means that the general trend showed the error to be 21%.

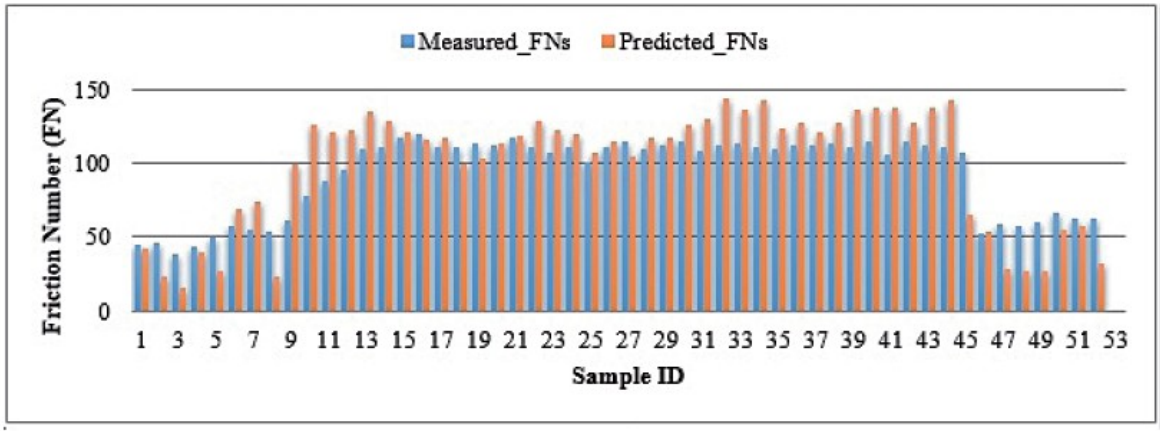


**Figure 56. Comparison between the measured and predicted FN's [ CITATION LiL16 \l 7177 ]**

When this is compared to the tread of tyre evaluated in this study, which has a ± 6% error on the flat concrete block. It could be said that from a single tread to a whole tyre the difference is 15%.

# Chapter 4: Conclusion and Recommendations

## 4.1 Macro texture

The DIC was used to create the macro texture road profiles of the Belgian paving that represent the rough road, over which the simulations were performed. Firstly the quarter car model was used to evaluate the effect of the tyre resolution, speed and road resolution on the tyre road contact. When the speed was increased for the model driving over the road, it was found that the difference in the tyre forces between the 1x1mm and the 15x15mm resolutions were less than 5%. This indicated that an increase in speed had little to no effect on the simulation of the tyre forces. When the tyre resolution was halved and doubled, the percentage error was also found to be less than 5%, which is considered negligible. It is preferred to use the recommended resolution by Cosin. When the road resolution was evaluated, it was determined that the normal force showed the largest increase in percentage error as the resolution increased (22%), which is considered significant. The lateral force also changed significantly (16%). The longitudinal force differed with less than 10%, and the moments by less than 5%. It can thus be concluded that the normal and lateral forces are mainly influenced by the change in road resolution for a quarter car.

The experimental and simulation results were also compared for the full-scale model to determine the optimum road resolution. The 1x1mm and 5x5mm road resolution indicated the same results, accept for the aligning torque (Mz), that had a very small percentage error of 1% between the results. Thus, it can be concluded that for the 1x1mm road resolution has no benefit on full scale simulations, especially when considering the simulation time due to the processing of a large amount of data points. The 1x1mm road resolution resulted in double the solving time of the 5x5mm road resolution. The percentage error of the simulation data of the various resolution as compared to the experimental data and differed with ± 26%, which indicated that the Adams model was sufficiently accurate and could represent the experimental setup. The percentage error difference between the ranges of road resolution resulted in a mere ± 2% and 5% for the normal force. From this, it was concluded that the change in road resolution did not have any significant effects on the simulation data when it was compared to the experimental data for the full-scale model. Since Cosin's claim was made on comparing the simulation data to each other, this was also investigated for the trailer driving over the Belgian paving. In general, the percentage error difference was much larger than that of the comparison of the experimental data, with a value of ± 6% for the full-scale model.

When the simulation is compared to the 1x1mm resolution, the normal force (7%) and aligning torque (12%) had the largest percentage errors for the full-scale model. The quarter car correlates with the 22% for the normal force and 16% for the lateral force. It was determined that the overturning moment results were the least sensitive to the change in a macro texture and the normal force was influenced the most for both models. Cosin's statement in the introduction has been proven to be true, that there are in fact a difference in the resulting forces and moments when the road resolution is changed, however the amount of percentage error was exaggerated and found to be less extreme than originally anticipated. Thus, the road resolution of 15x15mm is more than sufficient for simulations of full vehicle dynamics. The ±10 error is more than acceptable especially when the computational time was taken into account. The 10x10mm resolution should be considered for simulations of the quarter car, to ensure that the percentage error stays below 10%.

## 4.2 Micro texture

Various methods were used to determine all the unknown properties of the tyre and the road to be able to use the Heinrich/Klüppel model to estimate the friction coefficient. The experimental friction coefficient was determined through the use of Da Vinci's model, by dragging a single tyre tread block over different surfaces at several speeds. The surface height was measured with a laser and this was limited to a 0.12mm resolution to create a topography that represented the detailed asperities of the micro texture. This was sub sampled to evaluate the friction estimation over a rough road.

One significant aspect to the friction coefficient estimation, was the flash temperature. This influences the friction significant as mentioned in the literature study. Both surfaces evaluated indicated that as the vertical displacement and velocity increased, so did the change in temperature. The flat concrete block reflected a much higher average change in temperature (± 20˚C) compared to the tests over the Belgian paving (± 5˚C). The lower change in temperature over the rough road was caused by the tyre tread not being in constant contact with the surface, because the Belgian paving is very course with the multiple deep valleys allowing the tread to cool down as it moves across the surface.

To validate the friction coefficient model could be used on any surface, the flat concrete block was evaluated. It was found that the estimation showed a good correlation tot the experimental results with a percentage error difference of ±2%. The estimation had a percentage error of the ±6%. As expected, due to the higher frequency content of the rough road, the Belgian paving friction coefficient estimation had a percentage error of ±26%. When the estimation was compared to the experimental data, it varied by only ±10%. Thus validating that the Heinrich/Klüppel model can be used to estimate the friction coefficient with the relative accuracy on any class road. Both road classes indicated a decrease in percentage error when the displacement was increased, and the results were not dependent on the change in speed.

The percentage error for both the flat concrete and the Belgian paving increased as the road resolution increased, even though it fluctuated over the range of speeds. The percentage error increased with ± 10% when the road resolution was increased from 0.12mm to 0.24mm for the Belgian paving and 5% for the flat concrete block. This seems like an irrelevant amount, however when the graphs of these results were investigated in detail, it showed that the 10% increase could have a large effect on the friction coefficient for the Belgian paving. This small amount could result in large effects in full vehicle dynamic simulations. It was concluded that a road resolution larger than 0.144mm for the Belgian paving and 0.216mm for the flat concrete would result in inaccurate data.

## 4.3 Conclusion

The introduction mentions that the normal force influences the macro texture; this was evident from the percentage errors for the change in road resolution. The largest percentage error of the forces was seen for the normal force for both the quarter car and the full-scale model when simulations were compared to simulation. The macro texture change had little to no effect on the simulations of the full-scale vehicle model when the results were measured in a resolution smaller than 15x15mm. For the quarter car, a resolution of 10x10mm should be considered if simulations with less than 10% percentage error is required. The macro texture possibly has a larger influence on the quarter car dynamics since it becomes unstable at high speeds and more reliant on the normal force. These road resolutions were found to result in the most accurate simulation results, while speed and tyre resolution within the ranges evaluated had little to no effect on the results.

The micro texture effects friction coefficient in the form of lateral and longitudinal forces, which is evident from the effects that the road resolution has on the friction estimation. A change in the micro texture resolution had a more significant effect than the macro texture changes. It was established that a

smooth road should not be sampled at a resolution larger than 0.216mm and a rough road resolution limited by 0.144mm. The estimation increased as the vertical displacement increased, while the velocity had little to no effect.

## 4.4 Recommendations

The macro texture and how it affects the forces and moments at the contact patch has been evaluated thoroughly. The optimum macro texture road resolution is determined as 15x15mm for most vehicle model simulations, the only exception being a quarter car model that should be measured at 10x10mm. Furthur investigation could be implemented in looking at even larger resolutions and where the limit is for certain types of vehicle simulations

Since it was determined that the Heinrich/Klüppel model could be used to estimate the friction coefficient over a rough road with relative accuracy, it could be used in the future to simulate the road/tyre interaction with more certainty. Further investigation is however required into applying this model into a full scale tyre model while it rolls over a rough road, not just on a single tyre tread. It can now only be assumed that the full tyre has a 15% larger error than for the single tread. It is recommended that the complete Belgian block is evaluated and the friction coefficient determined with the use of the micro texture optimum resolution of 0.144x0.144mm. The friction coefficient can then be subsampled to a macro scale of a 15x15mm resolution. The road profile used for simulations can then consist of x, y and z coordinates with an additional matrix to represent the friction coefficient for each macro resolution point. When this can be incorporated into simulations, the contact patch can be represented in a more accurate manner when simulating vehicle dynamics.

# Appendix A: Camera specifications

## A.1 FLIR Lepton Camera

The FLIR Lepton was used to take thermal images of the tyre before and after friction estimation tests to be able to implement flash temperature effects. The camera comprises of the following properties in Table 10 [CITATION Unk15 \l 7177 ].

**Table 10. Specifications of camera used to take thermal images**

| Specification | Specification value |
|---|---|
| Resolution | 80x60 |
| **Spectral range [µm]** | LWIR 8-14 |
| **Pixel size [µm]** | 17 |
| Frame rate [Hz] | 8.6 |
| Thermal Sensitivity [mK] | <50 |
| FOV-horizontal | 51˚ |
| FOV-vertical | 63.5˚ |
| Depth of field [cm] | 10 to infinity |

## A.2 FLIR ThermaCAM camera

The FLIR ThermaCAM E2 camera were used to calibrate the FLIR Lepton camera since it provides direct values to specific areas on the image with the specifications indicated in Table 11 [ CITATION FLI02 \l 7177 ].

**Table 11. Specifications of camera used to calibrate the FLIR Lepton**

| Specification | Specification value |
|---|---|
| **Temperature range [˚C]** | -20-250 |
| **Spectral range [µm]** | 7.5-13 |
| **Accuracy [˚C]** | ±2 |
| **Thermal Sensitivity [˚C]** | 0.12 |
| FOV-horizontal | 19˚ |
| FOV-vertical | 25˚ |

## A.3 DIC Camera

The Point Grey Chameleon CMLN-13S2C-CS cameras were used with Fujinon DF6HA-1B lenses to create a road profile to determine the most accurate road resolution. A view main specification for the camera are shown in Table 12 [ CITATION The15 \l 7177 ].

**Table 12. Specifications of camera used to create road profile**

| Specification | Specification value |
|---|---|
| Resolution | 1296x964 |
| Frame rate [FPS] | 18 |
| Megapixels [MP] | 1.3 |
| **Pixel size [µm]** | 3.75 |
| Sensor format | 1/3'' |
| Exposure range | 0.01ms to 10s |

# Appendix B: Laser specifications

The Acuity AR700-8 was used to measure the road surface for the road friction estimation purposes. The specifications significant to this laser can be seen in Table 13.

**Table 13. Specifications of laser used to create topography for concrete block and Belgian paving**

| Specifications | Specification value |
|---|---|
| Span [mm] | 203.2 |
| **Resolution [µm]** | 10.2 |
| **Laser spot size [µm]** | 120 |
| Laser class | 3R |
| Sample rate [Hz] | 0.2-9400 |

# References

- Aavik, A., Kaal, T. & Jenston, M., 2011. *Use of pavement surface texture characteristics measurement results in Estonia*, Tallinn: Tallinn University of Technology.

- Acuity, 2015. *AR700 Laser displacement sensors*, Oregon: Schmitt Industries.

- Almohanna, I., 2017. *Skid resistance British Pendulum Tester and Full scale tire friction test*, Riyadh: King Saud University.

- American Institute of Physics, 2015. *Phys org*. [Online]
Available at: https://phys.org/news/2015-05-simple-leonardo-da-vinci-combined.html
[Accessed 14 May 2018].

- Becker, C., 2008. *Profiling of rough terrain*, Pretoria: University of Pretoria.

- Bosch, H.-R. B., Hamersma, H. A. & Els, P. S., 2016. *Parameterisation, validation and implementation of an all-terrain SUV FTire tyre model*, Pretoria: University of Pretoria.

- Botha, T. R., 2015. *Digital image correlation: Applications in vehicle dynamics*, Pretoria: University of Pretoria.

- Callum, 2016. *Skid resistance British pendulum tester and full scale tire friction test*. [Online]
Available at: http://slip-testing.co.uk/2016/08/11/british-pendulum-skid-resistance-test-work/
[Accessed 1 June 2019].

- Els, P., 2012. *Wheel Force Transducer Research and Development*, Pretoria: University of Pretoria.

- FLIR, 2002. *ThermaCAM*, Burlington: FLIR Systems Incorporated.

- FLIR, 2015. *Digi-Key*. [Online]
Available at: https://www.flir.com/globalassets/imported-assets/document/lepton-engineering-datasheet---without-radiometry.pdf
[Accessed 12 June 2018].

- Gibbs, J. H., 2015. *Polymer properties database*. [Online]
Available at: http://polymerdatabase.com/polymer%20physics/GlassTransition.html
[Accessed 26 July 2018].

- Gillespie, T. D., 1992. *Fundamentals of vehicle dynamics*. 1 ed. Warrendale: Society of Automotive Engineers.

- Gipser, M. & Hofmann, G., 2014. *FTire: High-end tire model for vehiclas simulation SIMPACK*, s.l.: COSIN scientific software.

- Hutchings, P. I., 2016. *University of Cambridge*. [Online]
Available at: http://www.eng.cam.ac.uk/news/leonardo-da-vinci-first-systematic-study-friction
[Accessed 28 November 2018].

- International Organization for Standardization, 1995. *Mechanical vibration. Road surface profiles. Reportinf of measured data*, Geneve: International Organization for Standardization.

- Kanafi, M. M., 2017. *Rocky road-surface roughness impacts on rubber friction*, Aalto: Aalto University .

- Lakes, R., 2009. *University of Wisconsin*. [Online]
Available at: http://silver.neep.wisc.edu/~lakes/VEnotes.html
[Accessed 7 October 2017].

- Li, L., Wang, K. C. & Luo, W., 2016. *Pavement friction estimation based on the Heinrich/Kluppel model*, s.l.: creative commons attribution.

- Michelin, 2018. *Monro muffler/brake and service*. [Online]
Available at: http://www.monro.com/datasheets/Michelin-LTX-A-T2.pdf
[Accessed 12 June 2018].

- Persson, B., 2001. Theory of rubber friction and contact mechanics. *Journal of chemical physics*, 115(8).

- Persson, B., 2006. Rubber friction: role of flash temperature. *Journal of Physics Condensed Matter*, pp. 7789-7817.

- Peterson, E., 2014. *Tire-Road friction coefficient estimation using a multi-scale,physics-based model*, Blacksburg: Virginia Polytech Institute and State University.

- Rao, S. S., 2011. *Mechanical vibrations*. 5th ed. Singapore: Pearson Education South Asia .

- Siewe, M. S., 2010. Resonance, stability and period-doubling bifurcation of a quarter-car model excited by the road surface profile. *Elsevier*, 10(1), p. 1016.

- Stallmann, M. J., 2013. *Tyre model verification over off-road terrain*, Pretoria: University of Pretoria.

- Teneerananon, P. & Yandell, W. O., 1980. *Microtexture roughness effect on predicted road-tyre friction in wet conditions*, Kensington: University of New South Wales.

- Unknown, 2016. *Armscor*. [Online]
Available at: http://www.armscor.co.za/?page_id=3967
[Accessed 1 June 2019].

- Unknown, 2016. *OpenCV*. [Online]
Available at: http://docs.opencv.org/2.4/doc/tutorials/calib3d/camera_calibration/camera_calibration.html
[Accessed 18 November 2016].

- Zuraulis, V., Van der Merwe, N. A., Scholtz, O. & Els, P. S., 2017. *Modelling and validation of testing trailer dor ABS and tyre interaction on rough terrain*, Budapest: ISTVS.